Fakultät für Medizin der Technischen Universität München

3D Cardiac Tissue Engineering for Studying Hypoplastic Left Heart Syndrome and other Disease Phenotypes

Christine Maria Poch

Vollständiger Abdruck der von der Fakultät für Medizin der Technischen Universität München zur Erlangung des akademischen Grades einer Doktorin der Medizin (Dr. med.) genehmigten Dissertation.

Vorsitzender: Prof. Dr. Wolfgang Weber

Prüfende der Dissertation:

1. Prof. Dr. Alessandra Moretti

2. Prof. Dr. Susanne Kossatz

3. Prof. Dr. Lars Mägdefessel

Die Dissertation wurde am 24.8.2020 bei der Technischen Universität München eingereicht und durch die Fakultät für Medizin am 15.02.2022 angenommen.

This thesis is dedicated to Felix.

INDEX

1 ZUSAMMENFASSUNG

Seit Beginn der erfolgreichen Differenzierung von humanen induzierten pluripotenten Stammzellen (hiPSC) zu Kardiomyozyten (hiPSC-CM) wurde eine neuartige molekulare Untersuchung verschiedenster genetischer Mutationen im Kontex von intakten, lebenden humanen Zellen möglich, welches das Krankheitsverständnis vertieft und die Identifizierung pathophysiologischer Vorgänge unterschiedlichster kardiovaskulärer Erkrankungen ermöglicht hat.

Das hiPSC-CM Zellmodell bietet sich auch für die Erforschung von kongenitalen Herzerkrankungen an. Diese sind meist heterogene Krankheitsentitäten, die kardiovaskuläre Malformationen während der embryonalen Entwicklung umfassen und die unterschiedlichsten Mutationen und klinischen Ausprägungen beinhalten. Zu dieser Gruppe zählt auch das hypoplastische Linksherzsyndrom (HLHS). Hierbei handelt es sich um eine kongenitale kardiale Malformation, bei der das Herz aus einer einzigen Kammer besteht, die für die Kreislaufversorgung verantwortlich ist. Diese Kammer wird dabei klassischerweise vom rechten Ventrikel gebildet, da der linke Ventrikel nur hypoplastisch und weitestgehend funktionslos angelegt ist. Der zugrunde liegende Pathomechanismus sowie eindeutige krankheitsverursachende Mutationen sind noch nicht im Detail erforscht, weshalb verschiedenste Hypothesen zum Pathomechanismus des HLHS bestehen.
Durch die molekulare Aufarbeitung verschiedener HLHS-Patienten im hiPSC- Modell konnte bereits ein besseres Verständnis der Zelldefekte erzielt werden. Nichtsdestotrotz ist die Erforschung des Krankheitsphänotypes dadurch limitiert, dass hiPSC-CM einen imaturen Phänotyp besitzen, der nicht alle Funktionen von reifen Kardiomyozyten rekapitulieren kann.

In der für diese Arbeit durchgeführte Studie wurden hiPSC von gesunden Probanden sowie drei verschiedene HLHS-Patientenlinien erfolgreich zu Kardiomyozyten differenziert. Auf der Basis von dezellularisiertem Primaten-Myokard wurde anschließend ein 3D-Herzpatch generiert, das eine verbesserte Maturierung der Zellen ermöglicht. Zudem wurden die 3D-Herzpatches unter physiologischer Vorspannung kontinuierlich elektrisch stimuliert. Diese biomimetische Kultur konnte signifikante Unterschiede zwischen Patienten und Kontrolllinien hinsichtlich Kontraktilität, Stimulierbarkeit und Zellidentität zeigen und stellt somit ein valides und wertvolles Tool zur besseren Erforschung unterschiedlicher Krankheiten dar.

2 ABSTRACT

Congenital heart diseases are a difficult target for clinical and developmental studies. Particularly, the investigation of pathophysiologic changes in early stages of cardiogenesis is vastly limited because of the restricted access to patient material at different stages of human development.
The advent of hiPSC technology and the possibility of generating patient- specific hiPSC-cardiomyocytes solved the obstacles of limited tissue access to some extent, providing a new platform for molecular investigation.

Hypoplastic left heart syndrome (HLHS) is a congenital cardiac malformation in which the heart consists of a single pumping chamber responsible for the body circulation, consisting of the right ventricle, whereas passive venous flow to the lungs maintains the pulmonary circulation.

In several hiPSC-CM models recapitulating common HLHS mutations, important findings suggest an underlying cell cycle defect and an immature phenotype of diseased HLHS cardiomyocytes (CM).
Nevertheless, a major drawback of hiPSC-derived cardiomyocytes (hiPSC-CM) is their lack of the mature subcellular organization, electromechanical properties, and three-dimensionality that are seen in differentiated human cardiomyocytes. These immature properties of standard-cultured hiPSC-CMs consequently limit the exploration of disease phenotypes.
In the current study, hiPSC-CMs were successfully seeded onto decellularized non-human primate ventricular myocardium (cECM), thereby generating 3D heart patches. By subjecting these 3D heart patches to specialized biomimetic culture conditions consisting of continuous mechanical preload and electrical field stimulation, a significant increase in structural and functional maturation of hiPSC-CM was achieved.
By partially overcoming the limitation of cellular immaturity, 3D cECM heart patches were generated from healthy and diseased hiPSC-CMs of three different HLHS patient lines.
The dynamic readout of contraction force and beating rate analysis revealed significant differences between patient and control lines in terms of contractility, excitability and cell type identity. This study demonstrates that certain disease phenotypes can only be recapitulated and investigated by a 3D biomimetic culture.

A.U.	arbitrary units
AIM1L	Absent in melanoma 1-like
BAI2	Brain-specific angiogenesis inhibitor 2
BDM	2,3-Butanedione 2-monoxime
BF	Brightfield
BMC	Biomimetic culture
BMCC	Biomimetic culture chamber
BMP	Bone morphogenetic protein
cECM	Cardiac extracellular matrix
ClCasp3	Cleaved caspase 3
CMP	Cardiomyopathy
CMs	Cardiomyocytes
CMW	Cardiac microwire
cMYC	Myelocytomatosis Viral Oncogene Homolog
cTNT	Cardiac troponin T
CTR	Control
DENND5B	DENN domain containing 5b
EB	Embryoid body
ECM	Extracellular matrix
EDTA	Ethylenediaminetetraacetic acid
EHT	Engineered heart tissue
FFR	Force-frequency relationship
FGF	Fibroblast growth factor
FGFR	Fibroblast growth factor receptor
GSK3b	Glykogen synthase kinase 3b
HCM	Hypertrophic Cardiomyopathy
hESC	Human embryonic stem cells
HIF	Hypoxia induced factor
hiPSC	Human induced pluripotent stem cells
hiPSC-CMs	Human induced pluripotent stem cell derived cardiomyocytes
IGF-1	Insulin growth factor 1
KLF4	Kruppel-like factor 4

LA	Left atrium
Lin28	Lin28 Homolog A
LV	Left ventricle
MACF1	Microtubule- actin crosslinking factor 1
MI	Myocardial infarction
MLC2a	Myosin light chain 2 atrial isoform
MLC2v	Myosin light chain 2 ventricular isoform
MLL1	Mixed lineage leukemia protein-1
mN	Millinewton
mRNA	messenger RNA
MYH	Myosin heavy chain
MYL	Myosin light chain
MYRF	Member myelin regulatory factor (MYRF)
NANOG	Nanog homebox
NDUFB10	NADH:ubiquinone oxidoreductase subunit B10
NHP	Non-human primate
OCT4	Octamer-binding transcription factor 4
OFT	outflow tract
PBS	Phosphate buffered saline
PBSCs	Peripheral blood mononuclear cells
PH	Phase contrast
RA	right atrium
RAB	Ras superfamily of small G proteins
ROCK	Rho-associated, coiled-coil containing protein kinase
ROI	Region of interest
RV	Right ventricle
SDS	Sodium dodecylphosphate
SEM	Standard error of the mean
SOX2	Sex determining region Y-box 2
SYBU	Syntabulin
TGFB	Transforming growth factor b
TRIS	Tris(hydroxymethyl)-aminomethan
TUNEL	terminal deoxynucleotidyl transferase dUTP nick end labeling
WNT	Wingless-Type MMTV Integration Site Family

4.1 HUMAN INDUCED PLURIPOTENT STEM CELLS (HIPSCS)

The first stages of human embryonic development are characterized by the presence of human embryonic stem cells (hESCs) that represent a population of pluripotent cells that have the capability to differentiate into various cell types with progressively narrower developmental potential. Their cellular and epigenetic programs gradually become less flexible and more defined, resulting in the acquisition of stable and tissue-specific phenotypes, building the basis of various tissues and organs of the human body.(Mali & Cheng, 2012)
In comparison, human induced pluripotent stem cells (hiPSCs) are cells derived from easily accessible somatic cells like fibroblasts, hair keratinocytes, peripheral blood cells, renal tubular cells or peripheral blood cells (Figure 1) that have been reprogrammed into an embryonic- like pluripotent state, providing an unlimited source of cells that can be differentiated into desired cell types.
HiPSC largely resemble human ESCs in terms of pluripotency, proliferation rate, self-renewal capacity, morphology, and cell- surface markers as well as epigenetic status, promoter and telomerase activities, and teratoma formation and, most importantly, their capacity to differentiate into any kind of somatic cell.(Ellen Poon, Chi-wing Kong, 2013; Takahashi et al., 2007; Yu et al., 2007)

4.1.1 GENERATION OF HIPSC

Because of their ability to differentiate into all somatic cell types as well as their unlimited self-renewal capacity, hiPSCs are a fascinating cellular system with great potential for clinical application. In the past 10 years, hiPSCs have become an increasingly interesting source for tissue regeneration, disease modeling, and drug screening platforms.(Hoekstra et al., 2012; Liang et al., 2013; Weinberger et al., 2018)

For in vitro studies, hESCs are isolated from human embryos in the blastocyst stage. Among other methods, they can be obtained from cryopreserved embryos created during in vitro fertilization(Lerou, 2011), which brings along many ethical concerns.

In contrast, hiPSCs can be generated by reprogramming adult somatic cells back into the stem cell state. By identifying the key regulatory genes expressed in pluripotent cell lines and

inducing a forced expression of these defined reprogramming factors, Takahashi and Yamanaka were the first ones to describe and generate human induced pluripotent stem cells and made them an applicable research tool.(Takahashi et al., 2007)

In principle, all cell types can be used as a source for hiPSC generation, as reprogramming is not limited to a specific cell type. Because of their easy accessibility, skin fibroblasts were the first cells used(Takahashi et al., 2007), while other cell types, such as peripheral mononuclear hair keratinocytes, renal tubular epithelial cells or peripheral blood mononuclear cells have been successfully used in later studies.

There are different approaches to induce the forced expression of the pluripotency genes including integrating methods that are based on transgene delivery, using vectors that result in the insertion of genes into the host genome (Figure 1).
These transgenes are usually introduced by modified lentivirus or retrovirus. However, the manipulation of the host cell genome that occurs limits the clinical application of the likewise created hiPSC. For this reason, alternative cellular reprogramming methods that do not permanently modify the host genome have been developed, called integration free methods that achieve xeno-free conditions for cell reprogramming (Figure 1). With the usage of a viral RNA vectors, episomal plasmids, piggyBac transposons or microRNAs no transgenes are introduced in the host genome. Lieu et al. established a commonly applied approach with the usage of an RNA sendai virus vector, which does not integrate transgenes into the host genome, that could now facilitate iPSC usage in clinical studies.(P. T. Lieu, 2015)

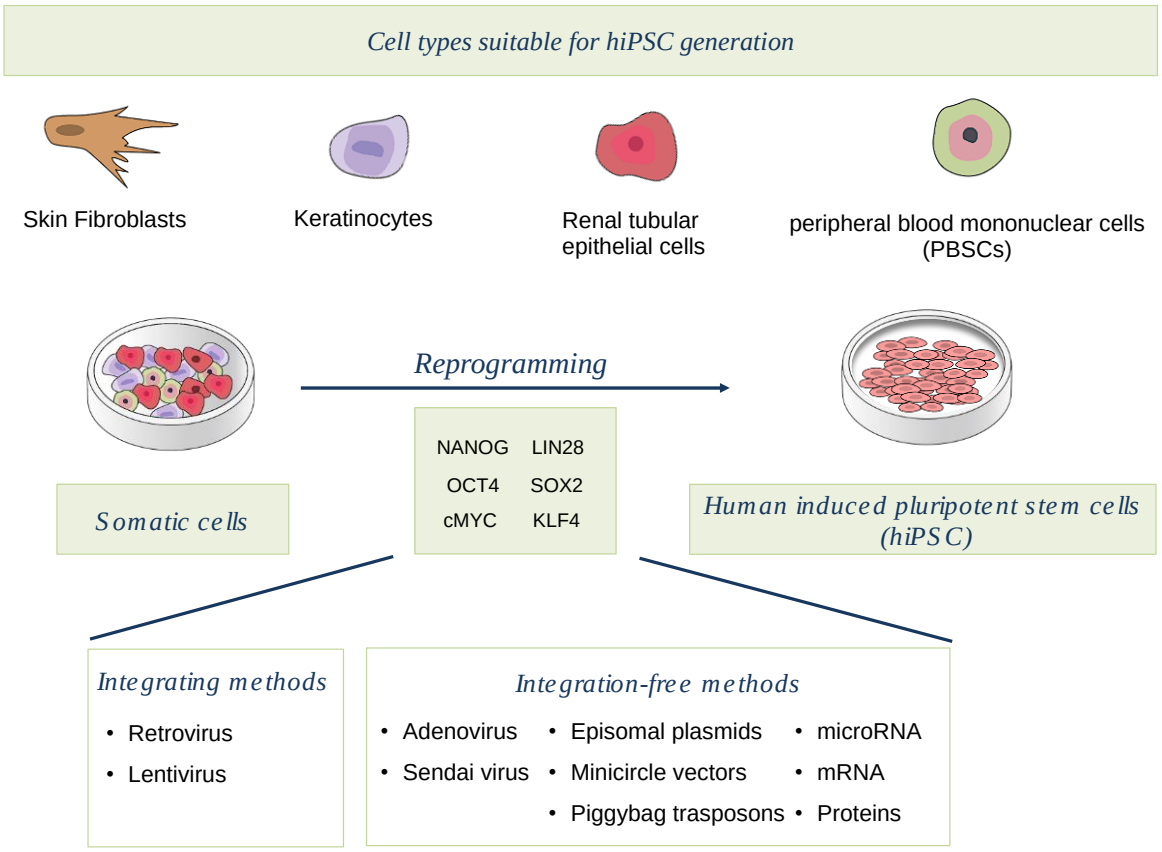

Figure 1. Generation of human induced pluripotent stem cells (hiPSCs). Cell types suitable for cellular reprogramming to hiPSCs are easily accessible cells like fibroblasts from skin biopsies, keratinocytes from hair, renal tubular epithelial cells obtained from urine, or mononuclear cells from peripheral blood.
Reprogramming of somatic cells to human induced pluripotent stem cells (hiPSC) is achieved by introducing several combinations of stem cell specific transcription factors (NANOG, OCT4, cMYC, LIN28, SOX2 and KLF4). Methods to induce this expression include integrating or integration- free methods.(Luna Simona Pane, Ilaria My, Alessandra Moretti 2016)

4.2 HIPSC-DERIVED CARDIOMYOCYTES (HIPSC-CMS)

Induced pluripotent stem cells hold developmental potential to differentiate into the advanced derivatives of all three primary germ layers.(Yu et al., 2007) Importantly, for the current study, hiPSCs can be differentiated into cardiomyocytes and cardiomyocyte-subtypes with nodal-, atrial-, or ventricular-like electrophysiological properties.(Ellen Poon, Chi-wing Kong, 2013; J. Zhang et al., 2009)

Specific signaling pathways controlling specification into the desired cell type during embryonic development are used to induce hiPSC differentiation. Cardiomyogenesis involves activin, Wnt, nodal, transforming growth factor β (TGF-β), and bone morphogenetic protein (BMP) signaling. Sequential upregulation and the defined inhibition of these signaling pathways mimics the physiological conditions in cardiomyocytic differentiation and lead to directed differentiation of hiPSCs into hiPSC-CM. (Figure 2). The differentiation of hiPSCs into the cardiovascular lineage was first introduced by Kattman et al.(Kattman et al., 2011) and further improved by their groups.(Willems et al. 2012)

Burridge et al. published a very reliable and highly efficient protocol for hiPSC-CM generation. It is based on small molecules modulating the Wnt pathway, namely, CHIR99021 and Wnt-C59, and can produce beating sheets of up to 90% cardiomyocytes.(Burridge et al., 2014)

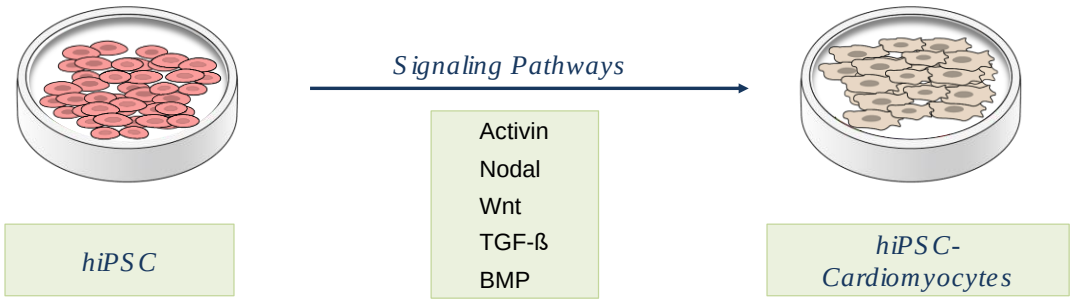

Figure 2. Differentiation of hiPSCs into hiPSC-CM. In vitro differentiation of iPSCs into hiPSC derived cardiomyocytes (hiPSC-CM) are based on temporal and dose-dependent modulation of specific signaling pathways that have pivotal roles during cardiovascular development (activin, nodal, Wnt, TGF- β, and BMP).

4.3 IMPORTANT HALLMARKS OF HYPOPLASTIC LEFT HEART SYNDROME

4.3.1 CLINICAL PHENOTYPE OF PATIENTS WITH HYPOPLASTIC LEFT HEART SYNDROME

Patients suffering from hypoplastic left heart syndrome display a crucially underdeveloped left ventricle together with a hypoplasia of the left ventricular outflow tract, the ascending aorta, and the aortic arch, often with additional aortic and mitral valve stenosis. In a normally developed heart, the left ventricle pumps oxygenated blood from the lungs through the aorta into the body, whereas the right ventricle pumps deoxygenated blood from the body into the lungs to be oxygenated (Figure 3).
In hypoplastic left heart syndrome, the rudimental left ventricle is unable to support systemic circulation. If untreated, HLHS accounts for 22% of deaths from congenital heart diseases in the first year of life.(Gillum, 1994)

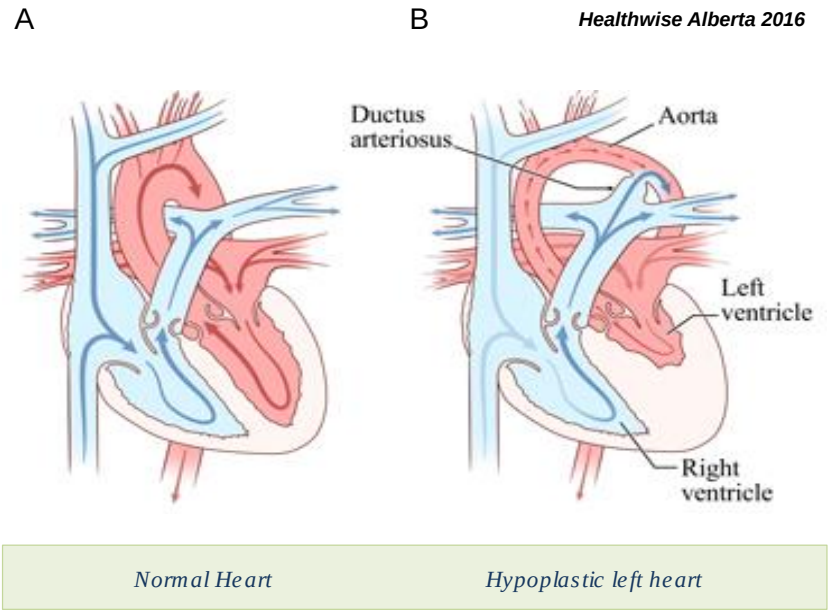

Figure 3. Structural differences between a normal heart and a hypoplastic left heart. **(A)** Morphology of a normal heart. **(B)** Schematic heart of HLHS patients with an underdeveloped left ventricle and aorta ascendens. (Healthwise Alberta 2016)

The HLHS phenotype usually appears in the early stages of cardiac development and is typically diagnosed in second-trimester ultrasound examinations.(Sadineni et al., 2017)
The incidence of the disease which comprises 4–8% of all congenital cardiovascular defects is approximately 1 in 10,000 live births. (Ferencz et al., 1985; Hoffman & Kaplan, 2002)

4.3.2 Long-Term outcome of patients with hypoplastic left heart syndrome

If untreated, HLHS is uniformly fatal. Although successful surgical intervention with functioning single-ventricle circulation dramatically improves survival, the 5-year survival-rate is still only 50–70% (Kern et al., 1997) and patients still suffer from lifelong impaired cardiac function and do not meet full life expectations.(Feinstein et al., 2012; Martin et al., 2017)
For this reason, it is essential to increase the knowledge and understanding of the disease-causing mutations and mechanisms underlying the HLHS phenotype to develop successful therapeutic approaches.

4.3.3 Current theories for underlying disease mechanisms in HLHS

Despite many studies, the molecular and physiologic defect underlying HLHS remain unclear and there are conflicting views regarding the role of flow, valvular, or myocardial abnormalities in its pathogenesis.(Crucean et al., 2017)

4.3.3.1 valve theory

Several studies in the past decade have focused on the so-called valve theory, which states that valvular dysplasia in HLHS is the cause of the clinical phenotype. It is postulated that fetuses with severe aortic stenosis at mid-gestation with co-existent left ventricular dilation or dysfunction and retrograde flow in the aortic arch progress to a HLHS phenotype until the time of birth. (Freud et al., 2014)
However, treatment attempts involving in utero fetal aortic valvuloplasty at mid-gestation have only partially achieved restoration of biventricular circulation in a small subset of patients, and treatment failed to ameliorate this phenotype sufficiently, disproving this theory as single causative of the HLHS phenotype.(Mäkikallio et al., 2006)

4.3.3.2 flow theory

Similar to the above-mentioned valve theory, the flow theory postulates that a lack of blood-flow- mediated physiologic remodeling impairs proper four-chambered heart formation. Abnormal flow patterns in the left atrium and pulmonary veins, as well as a monophasic

mitral inflow profile, are thought to be involved in the pathogenesis of the hypoplastic left ventricle formation.(Michelfelder et al., 2005)
In support of this theory, researchers generated the first models of a hypoplastic left heart in chick embryos by temporal disruption of the blood flow through the developing left ventricle.(Harh et al., 1973; Pesevski et al., 2018)
During early cardiogenesis, in the process of cardiac looping, asymmetric temporospatial flow dynamics occur. These flow profiles exert gradients of wall shear stress that lead to different expression patterns of shear-responsive genes. These facts favor the theory of the occurrence of morphological alterations of the heart in the setting of altered flow dynamics in the developing myocardium. However, the complex interplay makes it difficult to identify a certain pathway that can lead to the distinct phenotype of hypoplastic left heart syndrome.(Poelmann & Gittenberger-de Groot, 2018)

4.3.3.3 INTRINSIC CARDIOMYOCYTIC PROLIFERATION AND DIFFERENTIATION DEFECTS

Only recently, new studies have provoked a paradigm shift, stating that the complex phenotype of HLHS may arise in a combined manner from intrinsic cardiomyocytic defects resulting in left ventricular hypoplasia.(Liu et al. 2017)

A new animal study by Liu et al. aimed for recapitulating an HLHS phenotype in mutant mice using Sap130 and Pcdh9 gene mutations, identified by forward genetics, as disease causing. CRISPR-Cas9 genome editing showed that Sap130 mediates left ventricular hypoplasia and Pcdha9 increases penetrance of aortic valve abnormalities. These findings show that HLHS can arise from a combination of genetic alterations. Furthermore, an intrinsic cardiomyocyte proliferation and differentiation defect was observed. Particularly, TUNEL labeling showed an increase in apoptosis in the HLHS-LV but not RV tissue. Electron microscopy revealed a cardiomyocyte differentiation defect, with the HLHS-LV exhibiting short myofilament bundles with more branching and poorly defined Z-bands. This was associated with a mitochondrial maturation defect indicated by a low-density matrix, sparse cristae, and a reduction in mitochondrial size and shape. Although similar changes were observed in the RV, the changes were of lesser magnitude.(X. Liu et al. 2017)
Moreover, the observations of cell proliferation and differentiation defects were also recapitulated in a mouse iPSC-CM model generated from HLHS mutant mice fibroblasts

carrying the same mutations in the Sap30 and Pcdh9 genes, strengthening the postulated hypothesis.(X. Liu et al. 2017; Yagi et al. 2018)

5 HIPSC-CARDIOMYOCYTES: A CELL MODEL FOR IN VITRO DISEASE STUDIES

5.1 PATIENT-SPECIFIC HIPSC-CM

Congenital heart diseases are a difficult target for clinical and developmental studies. Particularly, the investigation of pathophysiological alterations in early phases of cardiogenesis is limited due to the restricted access to patient material at different stages of human development. The advent of hiPSC technology and the possibility of generating patient- specific hiPSC-CM solved the obstacle of limited tissue access to some extent, providing a new source of cells for molecular investigations.

Moreover, hiPSC technology opened up new possibilities for disease modeling in a patient-specific genetic background.(Moretti et al. 2010) Up to now, classical disease model systems, such as knockout animals, have been widely used, as mentioned above. Although these animal model systems are valuable tools for monogenic diseases, they fail to fully recapitulate clinical human phenotypes of complex genetic disorders and are further limited by fundamental developmental differences between species. (Krishnan et al., 2014)

The difficulty of creating genetic models of diseases that involve the enrichment of several mutations in genes crucial for cardiogenesis rather than a monogenic target highlights the advantage of patient-specific hiPSC in disease modeling. These cells harbor the whole set of genetic variants of an individual patient that ultimately results in the disease phenotype. Thus, hiPSC represent a promising tool to study the pathophysiological changes and different expression profiles induced by gene variants.
The aim of an ongoing study in our lab is to generate and characterize patient-specific hiPSCs from individuals suffering from hypoplastic left heart syndrome. Therefore, three patient iPSC lines with different identified de novo mutations were generated with the goal of uncovering novel molecular mechanisms that can be assigned to the onset of this complex genetic disease. After the successful reprogramming of patient skin fibroblasts into hiPSCs, the consecutive differentiation toward cardiomyocytes was used to study differences in the expression profiles and cellular physiology.

The first of the three de novo mutations (H1) selected for hiPSC-CM generation in this study is a mutation in the DENN domain containing protein 5B (DENND5B) gene, a protein involved in retrograde vesicular trafficking mediated by RAB proteins (Biesecker et al., 2009; Yoshimura et al., 2010) that are implicated in vesicular trafficking and endosomal degradation as well as two additional de novo mutations in syntabulin (SYBU) and brain-specific angiogenesis inhibitor 2 (BAI2), although the latter is predicted to be benign.

The second hiPSC line (H2) was generated from fibroblasts of a patient carrying disease-causing de novo variations in the MACF1 gene, a microtubule-associating factor, and myelin regulatory factor (MYRF), as well as predictably benign mutations in absent in melanoma 1-like (AIM1L) and NADH:ubiquinone oxidoreductase subunit B10 (NDUFB10). MACF1 is a microtubule actin crosslinking factor that is required for ciliogenesis (May-Simera et al., 2016), vesicle transport (Burgo et al., 2012), and autophagy (Morelo and Franco 2019).
The third HLHS hiPSC line (H3) represents a mutation in the fetal-growth-factor-receptor 1 (FGFR1) (H3), which was identified in a patient carrying an additional mixed lineage leukemia protein-1 (MLL1) mutation (Table 1).
In the following study, DENND5B, MACF1, and FGFR1, are considered as “lead de novo mutations”.

Cell line	*Sex*	*de novo Mutation*	*Gene description*	*Molecular function*
H1	m	DENND5B	DENN domain-containing protein 5B	Guanine nucleotide exchange factor for activation of RAB39 (Yoshimura et al., 2010) Implicated in vesicular trafficking and endosomal/autophagic degradation (Mignogna et al., 2015; Seto et al., 2013)
H2	m	MACF1	Mictotubule-actin crosslinking-factor 1	Ciliogenesis (May-Simera et al., 2016), vesicle transport (Burgo et al., 2012), and autophagy (Sohda et al. 2015)
H3	f	FGFR1	Fibroblast growth factor receptor 1	Growth factor for several cell types. Regulation of cilia length and function in various mammalian cells during embryonic development (Kunova Bosakova et al., 2019)

Table 1. *De novo* mutations selected for hiPSC-CM generation. The iPSC cell line H1 was generated from a male patient carrying the identified mutation in the DENN domain-containing protein 5B, a protein involved in retrograde vesicular trafficking mediated by RAB proteins. The iPSC cell line H2 was generated from a male patient carrying a "lead de novo mutation" in the microtubule-actin crosslinking-factor 1. Cell line H3 represents a female patient with a mutation in the fibroblast growth factor receptor 1.

5.2 EMBRYONIC STAGE OF HIPSC-CM LIMITS CLINICAL AND BIOLOGICAL APPLICATION

HiPSC-CMs have a significant value for in vitro disease studies and drug testing, and major steps have been taken toward the biological and clinical application of hiPSC-CMs. Especially in complex genetic diseases, hiPSC-CM models have unique advantages.

Nonetheless, there are some important features of 2D standard-cultured hiPSC-CMs that have to be considered. In particular, hiPSC-CMs have an immature phenotype. (X. Yang et al., 2014) Structurally, iPSC-CMs are smaller in size and have irregular cell shapes. Their sarcomeres are unorganized and the absence of T-tubules results in much slower excitation–contraction coupling.(Mummery et al., 2012; Tzatzalos et al., 2015)
Functionally, the electrophysiological characteristics of hiPSC-CMs are more heterogeneous than those of differentiated cardiomyocytes in human hearts. Mature ventricular CMs are electrically quiescent but excitable upon stimulation, whereas hiPSC-CMs exhibit spontaneous low-frequency contractions and immature characteristics with regard to their action potential.(Xiulan Yang et al., 2014)
For this reason, the improvement of hiPSC-CM maturation is essential for their application in complex disease studies such as HLHS.
Several promising approaches for the improvement of maturation (Figure 4) to overcome the limitations that hiPSC-CM immaturity bring along have been reported. (Xiulan Yang, Pabon, and Murry 2014; Tzatzalos et al. 2015; Tiburcy et al. 2017; Freytes et al. 2014; Ronaldson et al. 2018):

3D tissue engineering provides a 3D environment with appropriate stiffness and elasticity that improves cellular organization and can facilitate intercellular crosstalk, which influences CM differentiation and growth.(Zeevaart et al. 2009; Freytes et al. 2014, (Engler et al., 2009; Lundy et al., 2013) Additionally, the expression of cardiac contractile and gap junction

proteins is strongly promoted.(Feaster et al., 2015; Seth, 2013) Furthermore, hiPSC-CMs in 3D display an increase in mitochondrial mass and DNA which contributes to metabolic maturation.(Ulmer et al., 2018)

The application of **physiologic preload and electrical stimulation** are known growth stimuli. Physiological stretch promotes cell orientation and functional sarcomere alignment.(Matsuda et al., 2005; D. Zhang & Pu, 2018). Electrical conditioning by pacing-induced regular contractions leads to maturation of Ca^{2+} handling and contractile properties. Other signs of tissue maturation after electrical stimulation include an increased response to isoprenaline and decreased spontaneous beating activity. (Hirt et al., 2014; D. K. Lieu et al., 2013; Ronaldson et al., 2018) **3D- Bioprinting approaches** proofed additional benefits for cellular positioning with precise electrical and mechanical stimulation. (Cortes et al., 2020).

The substitution of neurohumoral factors such as the supplementation of the thyroid hormone or cortisol analogues showed that the number of ESC-derived CMs increases, followed by the upregulation of specific makers for cardiomyocytes. In addition, electrophysiological studies demonstrate more adult-like AP characteristics after free thyroid hormone (T3) supplementation.(Lee et al., 2010) Furthermore, the supplementation of FGF-1, IGF and VEGF vastly improves cardiomyocytic contractile performance. (Breckwoldt et al., 2017)

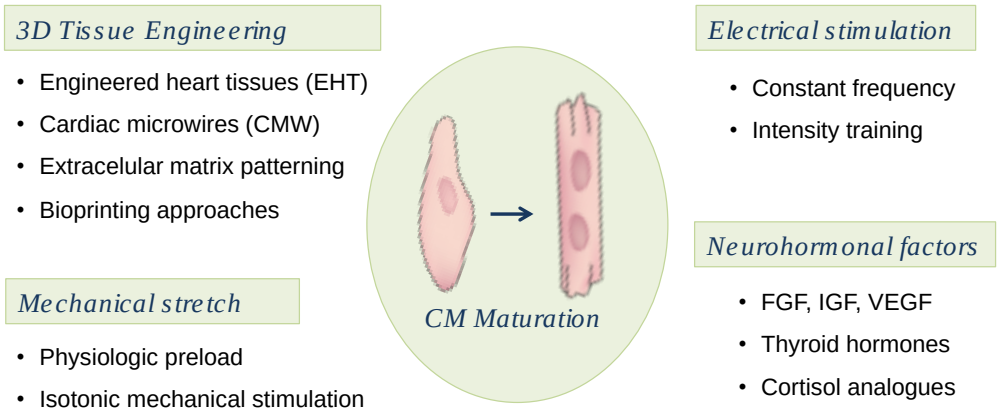

Figure 4. Maturational approaches for stem-cell-derived cardiomyocytes.
3D bioengineering approaches have shown to improve sarcomeric organization and contractile function by altering substrate stiffness. Furthermore, electrical/mechanical

conditioning and the administration of growth factors, hormones or cortisol analogues, substantially increase stem- cell derived cardiomyocyte maturation.

5.3 BIOENGINEERING HEART PATCHES USING EXTRACELLULAR MATRIX PROTEINS

Living cells and tissues can display high sensitivity to local molecular and topographic patterns, including those provided by complex and well-defined structures of the native cardiac extracellular matrix (cECM).(Stevens & George, 2005)

In the native human heart, cardiomyocytes are embedded in and surrounded by their natural environment, a stretch-sensitive network that is actively involved in the transduction of mechanical signals of cardiac cells.(Camelliti, Borg and Kohl 2005)
Single, isolated cECM components are readily available and frequently used for in vitro culture and are known for their beneficial effects on hiPSC-CM maturation. However, the potency of the cECM does not exclusively consist of isolated components; the functional interplay of mechanical properties and molecular cues make the cardiac ECM a unique culturing system. The fibrillar collagen meshwork of the cECM ensures the structural integrity of aligned myocytes.(Weinberger et al. 2018)
It provides a framework that translates cell contractions into the pumping movements of the heart.(Spinale, 2002) Additionally, it imparts the stiffness and compliance required for proper maturation and differentiation of myocytes.(Rodriguez et al., 2011) In fact, the microenvironment and stiffness of the ECM influences lineage specification in the stem cell state. (Engler al, 2005)
The biggest impact on maturation to date has been achieved by different approaches of 3D tissue engineering, such as the engineered heart tissue (EHT) consisting of a defined mixture of collagen, laminin or fibrinogen, hiPS-derived cardiomyocytes and fibroblasts.(Weinberger et al. 2018; Zimmermann et al. 2006; Tiburcy et al. 2017) After polymerization of the substrates, a surrounding matrix for hiPSC-CMs is created in which a high percentage of CMs changed their shape from round (typical for fetal CMs) to rod-like shaped (typical for mature CMs). Additionally, a more mature gene expression profile was observed.(Tiburcy et al., 2017)

5.4 3D cECM HEART PATCHES: A PROMISING SYSTEM FOR CARDIAC DISEASE STUDIES

With the advent of the hiPSC technology, new ways of disease study (Moretti et al., 2010; Chen et al., 2017; Dorn et al., 2018) and treatments (Mandai et al. 2017; Schwartz et al. 2015) have been paved and numerous studies have vastly increased our knowledge and understanding of hiPSC and hiPSC-derived cardiomyocytes (hiPSC-CM).

However, most of what we have learned so far is obtained from 2D culture; only recently has 3D culture in the cardiovascular field emerged as a widely used tool.(Tiburcy et al. 2017; Weinberger et al. 2018; Parsa, Ronaldson, and Vunjak-Novakovic 2015; Hansen et al. 2010)

With respect to the developmental features of the human heart, it can be assumed that cardiomyocytes require an environment in which they are firmly anchored and, at the same time, are able to contract without unphysiological resistance from the surrounding tissue. In this situation, not only do molecular cell signaling mechanisms play an important role but mechanical cues are also essential for proper cellular development and functioning. Tissue engineering methods can mimic an environment that favors the formation of intercellular connections and electrophysiological functioning.
Furthermore, fetal and immature properties of hiPSC-derived CM limit their utility for disease studies and drug testing. Reaching a more mature cellular state in a 3D context offers the opportunity to study disease phenotypes. With the application of physiologic preload and continuous electrical pacing, cardiomyocytes have to take over an active role and start generating directed force. This functional challenge which is existent in the 3D biomimetic cECM culture may provoke disease-specific defects that cannot be recapitulated in a 2D context.

5.5 HYPOTHESIS – 3D cECM HEART PATCHES: A PROMISING SYSTEM FOR CELLULAR HLHS PHENOTYPE ANALYSIS

In the current thesis, it is investigated whether hiPSC-CMs are able to integrate into a slice of decellularized non-human primate (NHP) cardiac extracellular matrix, generating a so-called 3D cECM heart patch. Cellular behavior inside this environment is analyzed and assessed to measure the improvement of function and maturation in customized biomimetic culture chambers (BMCCs).

Furthermore, patient-specific HLHS- iPSC-derived cardiomyocytes with identified lead de novo mutations in the genes MACF1, FGFR1, and DENND5B, are placed into the 3D cECM scaffold aiming to further mature hiPSC-CMs. Using the 3D cECM heart patches as a disease model allows the examination of key processes of disease dynamics and progression in the context of active cellular force generation and altered performance requirements.

MEDIA AND FACTORS USED:

2-Phospho-L-ascorbic acid trisodium salt	Ref: Sigma (49752)
Accutase	Ref: Gibco (A1110501)
B27 (-ins)	Ref: Thermofisher (A1895601)
B27 (+ ins)	Ref: Thermofisher (17504044)
BDM (2,3-butanedione 2-monoxime)	Ref: Sigmaaldrich (B0753)
Cell culture inserts	Ref: Sigma (PICM03050)
CHIR 98014	Ref: Sigma (SML1094-25 mg)
Collagenase type II	Ref: Worthington (CLS2)
DMEM-F12	Ref: Invitrogen (21331-020)
EDTA	Ref: Life technologies (15575-038)
Essential 8 (E8)	Ref: Invitrogen (A15169-01)
FBS	Ref: Invitrogen (10270)
Fluo-4 AM	Ref: Thermofisher (F14201)
Geltrex	Ref: Life technologies (A14133)
HBSS 10×	Ref: Invitrogen (14270)
Histoacryl	Ref: B.Braun (69390)
L-Glutamine	Ref: Invitrogen (25030)
Mounting medium	Ref: Dako (S3023)
Penicillin/Streptomycin	Ref: Invitrogen (15140)
Pluronic F-127	Ref: Sigma (P2443)
Rock inhibitor	Ref: Sigma (Y27632)
RPMI 1640 Medium	Ref: Life technologies (21875-034)
SuperFrost Ultra Plus Gold Adhesion Slides	Ref: Thermo Scientific (11976299)
Wnt C59	Ref: Sellek chemical (S7073 5mg)

6.1 CULTURE AND PASSAGING OF HUMAN INDUCED PLURIPOTENT STEM CELLS (HIPSCS)

Splitting

Guidelines and medium preparations (Burridge et al., 2014)

- HiPSCs were routinely maintained in stem-cell-maintaining medium E8 on Geltrex-coated Petri dishes (3.5 cm diameter) as colonies. To achieve cardiac differentiation, following the protocol of Burridge et al., cells needed to be adapted to single-cell culture for at least three passages prior to starting.
- Passaging solution: EDTA/NaCl solution. Add 500 µL of 0.5 EDTA and 0.9 g NaCl in 500 mL calcium/magnesium-free PBS (PBS (–)/(–)
- Geltrex-coated wells were equilibrated at room temperature for at least 30 min before usage.

Single-cell culture passage

On the day of passaging, differentiated colonies within the plate were removed by scratching them away. The cleaned plates, along with the remaining high-quality hiPSCs, were washed once with 2 mL of PBS (–)/(–) and then twice with 1 mL 2mM EDTA. After washing, 1 mL of EDTA solution was added and the plates were incubated at room temperature for 7–8 min. After the aspiration of EDTA, cells were resuspended with 2 mL of E8 supplemented with 2 µM rock inhibitor. Finally, cells were seeded into a new Geltrex-coated Petri dish (3.5 cm diameter). The splitting ratio was 1:10 with a cell number of 0.2-0.3 million cells/plate. Cells were supplied with E8 medium every day. After 5–7 days, cells reached 85–100% confluence and were ready to be passaged again.

6.2 DIFFERENTIATION OF HIPSCS INTO CARDIOMYOCYTES

Cardiac differentiation of hiPSCs

Sufficient cellular confluency of 80 – 90% for cardiac differentiation was usually reached 4-5 days after passaging. To start cardiac differentiation, according to the differentiation protocol by Burridge et al. 2014, confluent hiPSC were supplied with cardiac differentiation basic medium (RPMI 1640) supplemented with 6 µM CHIR98014 on day 0. After 2 days, medium was entirely exchanged to basic medium supplemented with 2 µM Wnt-C59. On differentiation day 4, cells were supplied with basic medium followed by medium exchange

every other day. Cells were expected to start beating between day 9-12 after initiation of cardiac differentiation. (Figure 5)

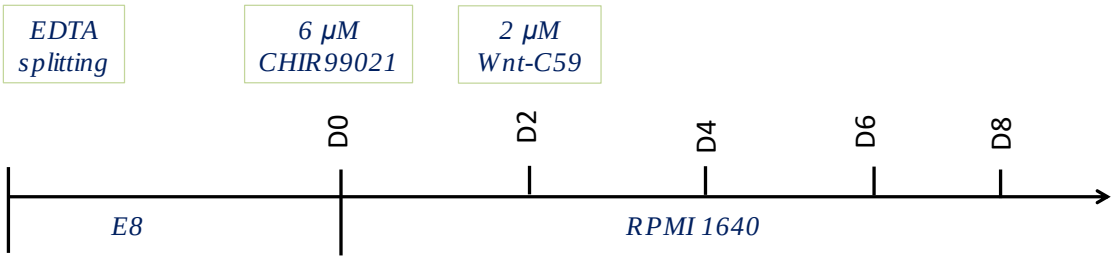

Figure 5. Chemically defined generation of beating hiPSC-derived cardiomyocytes by modulation of Wnt pathway. (Burridge et al.2014) Day 0 of differentiation is defined as induction of cardiomyocyte differentiation when sufficient cellular density is reached.

hiPSC-CM Purification and Preservation

For CM purification, beating sheets were manually cut under the microscope and transferred to fibronectin-coated 4-well plates between days 15-18. After replating of cells, medium was changed once a week.

6.3 DISSOCIATION OF HIPSC-CM

Contracting explants were placed in 1.5 mL of HBSS. As soon as the explants had sedimented to the bottom, all supernatant was removed. Afterwards, cells were suspended in 250 µL collagenase type II solution (480 U/ml collagenase type II suspended in 10 ml HBSS) for dissociation to single cells. Enzyme digestion was promoted during a 30 min. incubation period in the Thermomixer (37 °C, 850 rpm). Dissociated single cells within the solution were collected and placed into 20% Melton medium (E8 supplemented with 20% FBS; EB20) to stop collagenase reaction. The explants that had not yet been dissected were again suspended in 250 µL of collagenase type II with a 30 min incubation period in the Thermomixer (37°C, 850 rpm). This step was repeated until all explants were fully dissociated (up to 4 cycles).

After the last collagenase digestion cycle, the cell suspension was centrifuged for 5 min at 250–300 g and the supernatant was carefully removed, leaving a cell pellet at the bottom.

6.4 GENERATION OF 3D CECM HEART PATCHES

6.4.1 PREPARATION OF NATIVE NON-HUMAN PRIMATE HEART SLICES

For ex vivo heart slice preparation, non-human primate myocardial tissue was obtained from left mid-ventricular transmural sections that were immediately placed in a 30 mM 2,3-butadione-2-monoxime solution at 4 °C. The sections were embedded in 4% agarose and further processed to 1.0 × 0.5 cm x 300 µm thick myocardial tissue slices by vibratome cutting (VT1200S, Leica Biosystems, Germany) (Figure 6). NHP cardiac tissue samples were shipped to Munich from the "Deutsches Primatenzentrum Göttingen," where they were part of a vaccination study (Aktenzeichen: 33.19-42502-04-16/2264).

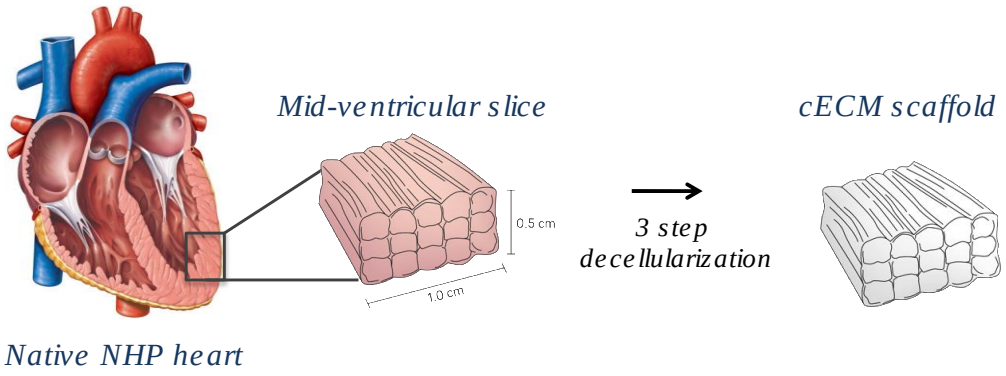

Figure 6. Generation of cECM scaffold. After left mid-ventricular transmural sectioning, vibratome cutting was performed to achieve tissue slices of of 300 µm thickness and dimensions of 1.0 x 0.5 cm. Tissue treatment with a modified version of the three-step protocol of Oberwallner et al.(Oberwallner et al. 2014) in which Tris and SDS was applied to achieve a cell-free cardiac ECM scaffold with preserved structure ready for reseeding with hiPSC-CMs.

6.4.2 DECELLULARIZATION OF NHP HEART SLICES

Guidelines and media preparations

Decellularization was performed according to a modified version of a three-step protocol described by Oberwallner et al.(Oberwallner et al., 2014)

Lysis buffer: 10 mM Tris suspended in 0.1% EDTA, pH 7.4
Solubilization solution: 0.5% sodium-dodecylsulfate (SDS) dissolved in PBS (–)/(–)
Protease inhibition: 50% FBS in PBS (-)/(-) overnight 4°C
Freshly cut myocardial tissue slices were washed twice with PBS (–)/(–) and incubated in Tris –based lysis buffer at room temperature for 2h on a rocking plate. Slices were then incubated in the SDS-based solubilization solution for 6h at room temperature on a rocking plate. After this step, samples were washed three times with PBS (+)/(+) for 10 min and incubated in protease inhibition solution overnight at 4°C. Samples were stored in PBS (+)/(+) with penicillin/streptomycin at 4 °C for up to two months before recellularization.

6.4.3 BIOPRINTING HIPSC-CM ONTO CECM TO GENERATE 3D CECM HEART PATCHES

Cardiac ECM scaffold slices were anchored in biomimetic culture chambers via small plastic triangles attached to the slices with tissue adhesive (Histoacryl) according to the fiber direction. The ECM scaffold was placed on a cell culture insert. With a bioprinting approach, a pluronic-based seeding frame was printed on the borders of the cECM scaffold to facilitate standardized and even seeding of hiPSC-CMs (Figure 7).

To prepare the printing material, 3.3 g of Pluronic F-127 (Sigma-Aldrich) was carefully mixed with 10 mL of sterile, filtered, deionized water and stored at 4 °C. For printing, the liquefied solution was filled into a 10 mL syringe connected with a 0.58 mm diameter standard Luer-Lock nozzle (Vieweg Dosiertechnik), placed into the pneumatic printhead, and tempered to 37 °C. The printing bed was heated to 40 °C to prevent the thermosensitive material from flowing away during the printing process. The seeding frame itself was printed directly onto the ECM sheet applying 1.41 bar extrusion pressure, a printing speed of 5 mm/s, and a layer height of 0.1 mm. A square with an inner edge length of 5 mm, a wall thickness of 1 mm, and a height of 3 mm was selected as a geometric design (Figure 7).

The cell pellet of dissociated iPSC-CMs was not resuspended with medium but directly pipetted stepwise with 4 µL cell solution/step on top of the matrix. Newly generated 3D heart patches were kept in EB20 medium for 2 days after seeding and were changed to RPMI+ B27 (-ins) after 2-4 days.

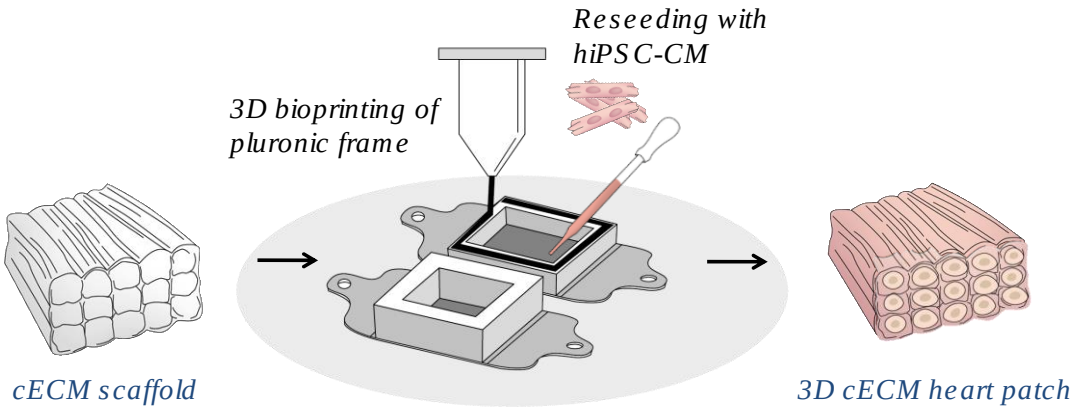

Figure 7. Generation of 3D cECM heart patches using a custom-made 3D bioprinting setup. Reseeding strategy of cardiac ECM scaffold with patient and control hiPSC-derived cardiomyocytes generating a 3D cECM heart patch, using a custom-built 3D printer with pneumatic printhead for the generation of standardized 3D cECM heart patches.

6.5 BIOMIMETIC CULTURE OF 3D CECM HEART PATCHES

In the first week after seeding, cells were allowed to sit and integrate into the matrix before the transferal to biomimetic culture chambers (BMCC). The medium was changed every other day underneath the filter. After observation of significant matrix movement by cellular contraction, 3D cECM heart patches were transferred to customized biomimetic culture chambers (Fischer et al., 2019) that allow the application of physiological preload together with continuous electrical stimulation.

For 3D cECM heart patch culture a constant preload of 1 mN together with electrical stimulation at 1 Hz (50 mA pulse current, 1 ms pulse duration) was chosen. Furthermore, the BMCCs enable a continuous readout of contraction force, beating rate, and excitability upon stimulation and facilitates analysis such as the force-frequency relationship during the whole period of 3D culture.

A total of eight biomimetic chambers are arranged on a system board with an integrated rocker plate (60 rpm, 15° tilt angle) placed in an incubator set at 37 °C, 5 % CO_2, 20% O_2, and 80% humidity. Individual stimulation impulses can be set for each of the eight chambers.

Via USB, the board is connected to a computer that serves as a graphic display and recorder for the obtained data and that executes freely programmable stimulation schedules.
These functions were implemented with a custom-written software utilizing the free library "Oscilloscope_DLL" (M. Bernstein) Contractility data were imported into and analyzed by "LabChart Reader" (ADInstruments) as described by Fischer et al. 2019.

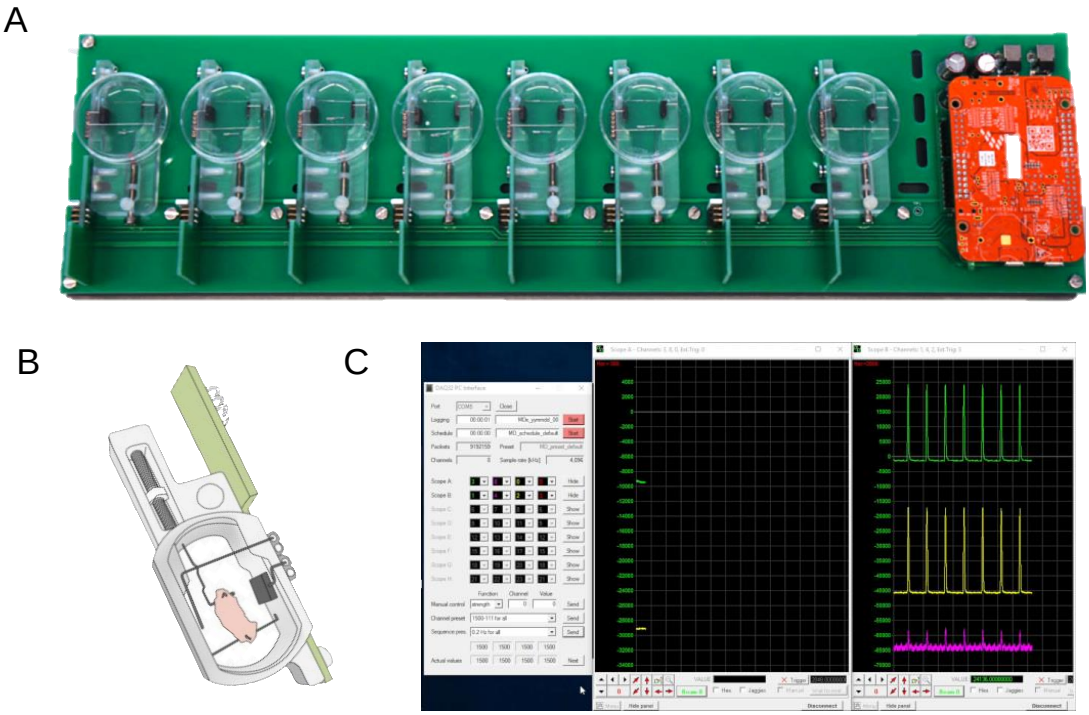

Figure 8. Biomimetic cell culture system. (A) Control unit composed of eight biomimetic culture chambers combined on a circuit board that can be operated in a standard CO_2 incubator. Signals from the magnetic field sensors are processed by a microcontroller that also provides bipolar stimulation pulses via a multiplexed current source. **(B)** Schematics of the culture chamber with attachment of 3D cECM heart patch via plastic triangles to a spring wire with magnetic tip. Changes in magnetic field are detected by an integrated sensor. Field stimulation is provided by graphite electrodes connected to a constant current pulse generator. **(C)** Signals from the magnetic field sensors are processed by a microcontroller that also provides bipolar stimulation pulses via a multiplexed current source. Data are transmitted via USB to an external PC for recording and scheduled execution of stimulation protocols.(Fischer et al., 2019)

6.6 LIVE/DEAD VIABILITY ASSAY

To dynamically evaluate cell viability during the culture period, cells were washed with PBS (+)/(+) twice before a 30 min incubation with ethidium dimer (4 µM) and calcein (2 µM) at 37 °C. After the patches were washed twice with PBS (+)/(+), patches were imaged under the fluorescence microscope (Leica DMI6000 B).

6.7 CALCIUM IMAGING OF 3D CECM HEART PATCHES

cECM heart patches were incubated in culture medium containing 2 µM Fluo-4-AM, 0,75% Kolliphor EL and 30 mM 2,3-butadione-2-monoxime to induce mechanical arrest, for 30 min at 37 °C, washed, and incubated for another 30 min at 37 °C in Tyrode's solution (135 mM NaCl, 5.4 mM KCl, 1 mM MgCl2, 10 mM glucose, 1.8 mM CaCl2, and 10 mM HEPES; pH 7.35**)** containing 30 mM 2,3-butadione-2-monoxime to allow de-esterification of the dye. Field stimulation was achieved with a customized setup using graphite electrodes connected to a stimulus generator (HSE Stimulator P, Hugo Sachs Elektronik, March-Hugstetten, Germany) providing depolarizing pulses (50 V, 5 ms duration) at 0.5-2.0 Hz as indicated. Calcium signals from the cECM heart slices were subsequently imaged in the above-mentioned medium conditions (Tyrode's solution supplemented with Ca^{2+} containing 30 mM 2,3-butadione-2-monoxime to induce mechanical arrest) using an upright epifluorescence microscope (Zeiss Axio Examiner) equipped with a 40x objective, a GFP filter set, and a Rolera em-c2 EMCCD camera.
Imaging settings (illumination intensity, camera gain, binning) were adjusted to achieve an optimal signal to noise ratio while avoiding pixel saturation. Imaging rates were 30 fps. ImageJ (National Institutes of Health, Bethesda, MD) was used to quantify fluorescence over single cells and over background regions. Subsequent analysis was performed in RStudio (RStudio Team (2015) using custom-written scripts. After subtraction of background fluorescence, the time course of Fluo-4 fluorescence was expressed either in arbitrary units or normalized to the initial value (F/F_0). After manual selection of the starting points and the peaks of the calcium transients, the transient amplitude and diatolic F/F_0 values were calculated.

6.8 CRYOSECTION AND IMMUNOFLUORESCENCE OF 3D CECM HEART PATCHES

Cryosection of 3D cECM heart patches was necessary for immunofluorescence analysis. Before freezing, the tissue was placed into a 30 mM 2,3-butadione-2-monoxime solution to induce mechanical arrest followed by 15 min incubation in 4% paraformaldehyde (PFA) at room temperature. Following a washing step with PBS (+/+) five times for 5 min, samples were placed into 10% sucrose solution overnight. Tissue samples were transferred to a standard cryomold and covered with the required amount of OCT solution.
The mold was then transferred to a glass dish filled with methylbutane and freezing was achieved by dipping the glass dish into liquid nitrogen. The frozen sample was cut into 16–18 µm sections collected on SuperFrost Ultra Plus Gold Adhesion slides using a standard cryostat (Leica).

After cutting, samples were allowed to dry on the cover slides for 30 min at room temperature before immunostaining. After washing with PBS (+/+) 5 times, cell permeabilization and blocking was accomplished with 0.1% Triton X100 and 10% fetal bovine serum (FBS) suspended in PBS (+)/(+) for 1 h of incubation at 37 °C. Primary antibodies (Table 1) were diluted to the desired concentration in 0.1% Triton X100 and 1% FBS suspended in PBS (+)/(+) and incubated for 2 h at 37 °C.
After incubation, samples were washed five times with 0.1% Triton X100 in PBS (+)/(+). Secondary antibodies (Alexa Fluor 488, 555, 594, and 647, 1:500, Thermo Fisher) of the appropriate species were diluted in the desired concentration in 0.1% Triton X100 and 1% FBS suspended in PBS (+)/(+) and incubated for 1 h at 37 °C.

After all steps of immunostaining were completed, samples were washed five times with 0.1% Triton X100 in PBS (+)/(+) and mounted with DAKO mounting medium. Images were taken using a DMI6000-AF6000 Leica epifluorescence microscope and a Leica confocal microscope (DMi8)

Reagent	Source	Reference	Concentration (application)
Anti-Cardiac Troponin T, mouse monoclonal	Thermo Fisher Scientific	MA5-12960	1:500 (IF)
Anti-MLC2a AF647, mouse monoclonal	Synaptic systems	311011 AT1	1:100 (IF)
Anti-MLC2v, mouse monoclonal	Synaptic systems	310111	1:100 (IF)
Anti-PH3, rabbit polyclonal	Millipore	06570	1:100
Anti-Cleaved Caspase 3, mouse monoclonal	R&D systems	MAB 707	
Anti- KI67, rabbit polyclonal	Abcam	ab15580	1:50 (IF)
Anti- Lamin B, rabbit polyclonal	Abcam	ab16048	1:100 (IF)
Cell Brite	Biotium	SKU30024	Assay instruction
LIVE/DEAD viability/cytotoxicity kit	Thermo Fisher Scientific	L3224	2 µM Calcein 4 µM EthD
Phalloidin (F-actin) AF647	Thermo Fisher Scientific	A22287	1:200 (IF)
Fluo-4 AM cell permeant	Thermo Fisher Scientific	F14201	2 µM (Calcium imaging)
TUNEL assay	Roche	12156792910	Assay instructions

Table 2. List of antibodies, fluorescent probes and assays

6.9 STATISTICAL ANALYSIS

Statistics were performed with online tools (http://www.socscistatistics.com). Data that passed tests for normality were analyzed with the use of t-tests for equal (Student's t-test). For data that were not normally distributed, a Mann–Whitney U test or chi-squared test was applied. P-values of less than 0.05 were considered statistically significant. Data are shown as means ± SEM, unless indicated differently.

7 RESULTS

7.1 GENERATION OF NHP CECM SCAFFOLDS

Native cardiomyocytes and other cell types from a 300 µm thick NHP LV slice were successfully removed using the modified three-step protocol developed by Oberwallner et al.,(Oberwallner et al., 2014) as mentioned in the methods section. Immunofluorescent analysis confirmed a cell-free matrix with negative DAPI staining. The results were directly compared to unmodified native tissue sections to verify acellularity (Figure 9).

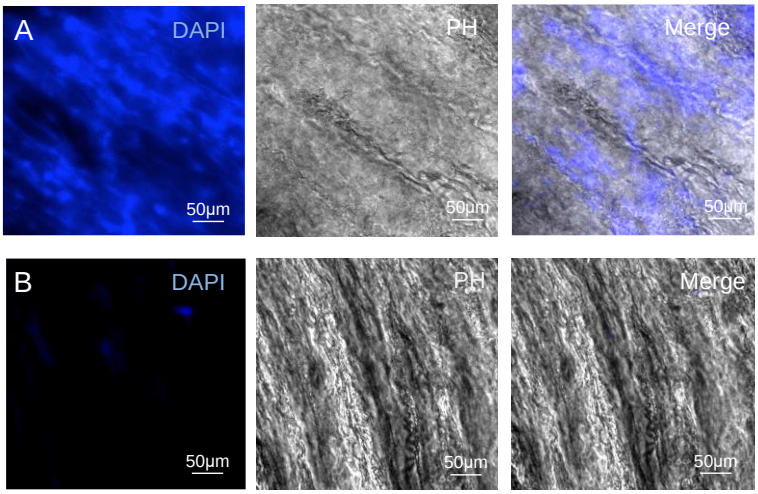

Figure 9. Generation of acellular NHP heart tissue. (A) native NHP heart tissue slice and **(B)** decellularized NHP heart tissue slice with DAPI stain for visualization of cell nuclei and phase contrast (PH) for analysis of tissue integrity.

7.2 SUCCESSFUL GENERATION OF STANDARDIZED 3D CECM HEART PATCHES

7.2.1 BIOPRINTING APPROACH FOR RESEEDING HIPSC-CMS ONTO CECM SCAFFOLD

With a bioprinting approach, a defined and standardized seeding frame for in vitro differentiated hiPSC-CM was printed on the borders of each cECM that had been previously anchored to plastic triangles for biomimetic culture chamber cultivation (Figure 10AB). The pluronic frame displayed stable geometry for about 24-36 h after printing, which was the ideal time window for hiPSC-CMs to attach to the matrix.

The reproducibility of the reseeding method was confirmed by consistently beating cardiac patches, that showed a high degree of cellular integration into the cECM, indicated by matrix movements and rate of cell survival.
Significant matrix movements were usually first seen between days 4 and 7 after reseeding. Subsequently, more and more matrix areas displayed movements translated by cell contraction, indicative of cell integration that was tracked with light microscopy during the time of biomimetic culture (Figure 10CD).

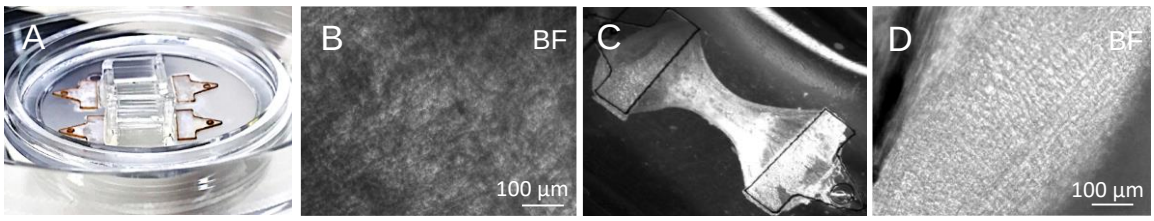

Figure 10. Bioprinting approach for seeding hiPSC-CM onto cECM patch. (A) Pictures of printed pluronic frame on cECM matrix patches prior to reseeding procedure with plastic triangles that serve as anchorage for BMCCs attached on both sides of the cECM. **(B)** Diffuse cellular integration and orientation of hiPSC-CM on Day 5 after reseeding in brightfield microscopic analysis on day 5. **(C)** hiPSC-CM integration into cECM network as indicated by the matrix modulation on day 15. **(D)** Cellular alignment and orientation with cECM scaffold on day 15 indicated by brightfield microscopy.

7.3 PROGRESSIVE INCREASE OF CONTRACTION FORCE OF HIPSC-CMS INSIDE 3D CECM HEART PATCHES

When sufficient cellular integration into the matrix scaffold was achieved (usually days 5–7 after seeding), 3D cECM heart patches were placed into the biomimetic culture chambers to allow dynamic quantification of contractile force. In the first 15 days after seeding, a continuous improvement of contractile performance was seen (Figure 11) with a maximum force amplitude of 2.1 mN and an overall average of 0.84 mN (± 0.081) on day 10, 1.20 mN (± 0.137) on day 20 and 1.59 mN (± 0.104) on day 40. (Figure 11)

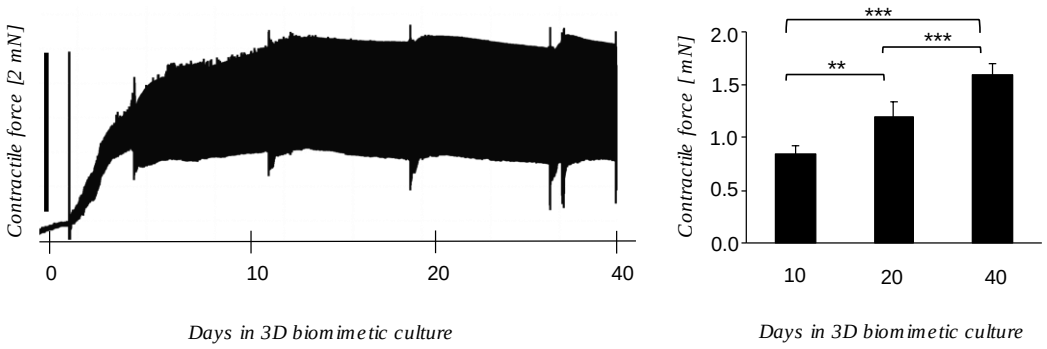

Figure 11. Contractile force analysis of 3D cECM heart patch within BMCCs.
Left**, r**epresentative contraction force plot of hiPSC-CM inside 3D cECM heart patch paced with 1 Hz throughout culture period of 40 days with statistical analysis (right). Data are shown as mean ± SEM, n= 7, ** $p \leq 0.05$ *** $p \leq 0.01$, t-test.

7.4 ENHANCED SARCOMERIC ORGANIZATION AND CELLULAR ALIGNMENT OF HIPSC-CM INSIDE 3D CECM HEART PATCH

In parallel to the functional maturation that the cells undergo, a similar improvement in structural maturation was observed with respect to cell alignment and elongation after 40 days when the cells were subjected to mechanical load and electrical pacing, as assessed by immunofluorescence analysis for cardiac troponin T and phalloidin. Most of the CMs inside the ECM displayed an elongated cell shape and aligned sarcomeres (Figure 12), whereas CMs in 2D culture still exhibited chaotic sarcomeric structures and variable cell sizes (Figure 12). Moreover, 3D-cultured hiPSC-CMs appeared to have thicker sarcomeres compared to their 2D control cells, which indicates a stronger myofibrillar development in the 3D culture system.

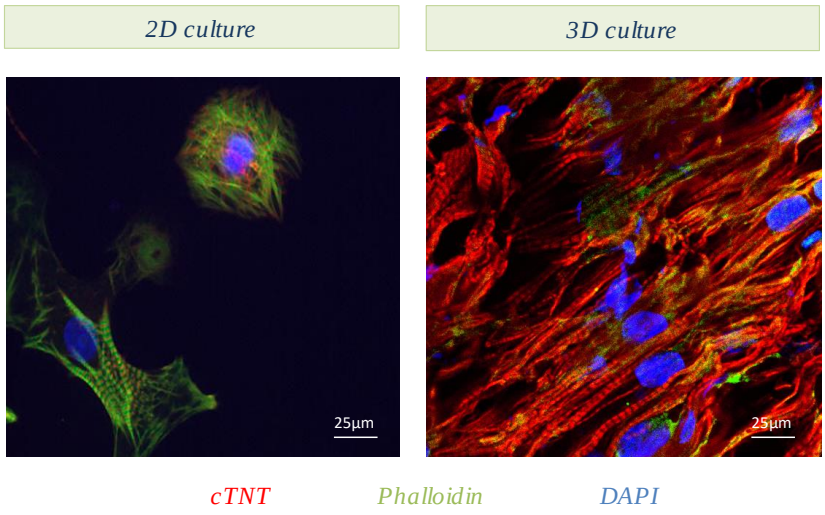

Figure 12. Improved sarcomeric structure of hiPSC-CM inside 3D cECM heart patches. HiPSC-CMs in standard 2D culture after 40 days showed irregular sarcomeric structure and cell size. CMs in 3D culture after 40 days exhibited elongated cell shape and sarcomeric organization.

7.5 DECREASED CONTRACTILE PERFORMANCE OF HLHS HIPSC-CMS IN 3D BIOMIMETIC CULTURE

Continuous monitoring of contractile performance starting on day 7 after reseeding of patient and control cell-lines, hiPSC-CMs within the biomimetic chambers showed that control cell lines exhibited an increase in contraction force during culture period with a maximum force amplitude of 1.8 mN on day 24 and an average of 1.32 mN (n = 6; 3 patches/cell line, ± 0.236, p = 0.17), whereas all three HLHS hiPSC-CM cell lines performed similarly with a gradual decline in contractile performance over time (Figure 13AB). The maximum contractile force was reached on day with 0.53 mN with an average of 0.43 mN ±0.025 (n = 9; 3 patches/cell line) and was significantly reduced already at the beginning of biomimetic culture on day 7 (HLHS 0.40 mN ±0.02 vs. CTR 0,71 mN ± 0.053, p<0.00001, t-test) with a further reduction by day 24 (HLHS 0.16 mN ± 0.023 vs.1.32 mN ±0.236, p<0.00001, t-test) (Figure 13B). Paceability and electrical coupling was simultaneously addressed during biomimetic culture. Over time, control cECM heart patches displayed a gradual electromechanical maturation at different stimulation frequencies from 0.2 Hz-1.5 Hz (Figure 13CD).
However, the percentage of HLHS cECM heart patches responding to frequencies higher than 0.5 Hz dropped significantly from 72.7 % ± 6.32 on day 7 to 9.1% ± 6.22 on day 24, ** p≤0.00001, t-test (Figure 13D). Correspondingly, control patches developed a positive force-frequency relationship on day 15 at frequencies between 0.5 Hz and 1.5 Hz whereas the HLHS patches failed to develop this functional phenotype but adapted a negative FFR. (Figure 13E)

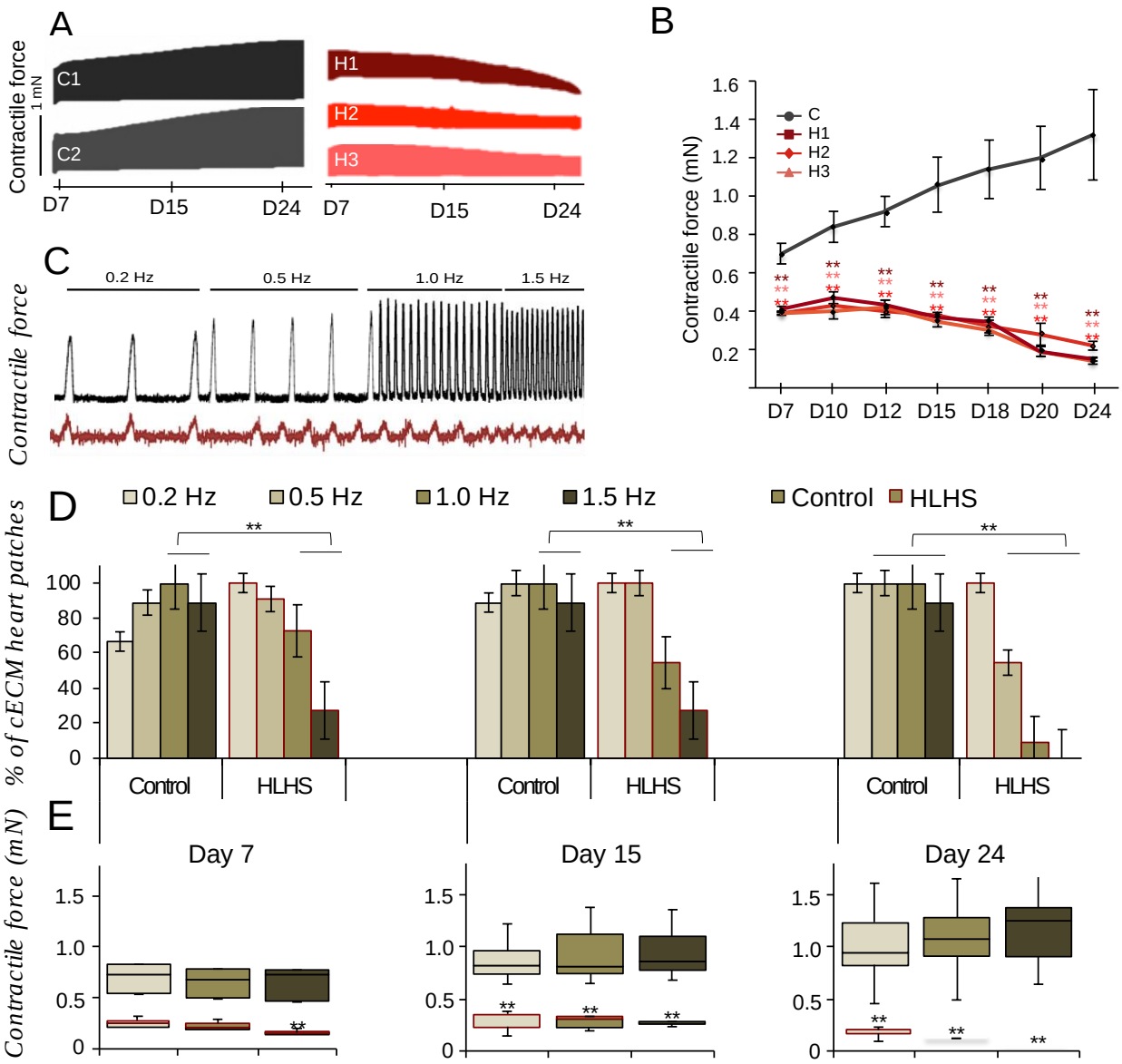

Figure 13. HLHS lines in 3D culture under electromechanical stress develop a reduced contractile force with negative force-frequency relationship. (A) Representative contraction force traces of control and HLHS cell lines within 3D cECM heart patches. **(B)** Statistical analysis of average contraction force (mN) on days 7, 15, and 22. Data are shown as mean ± SEM, n ≥ 3 patches/cell line, color-coded asterisks indicate significant differences (** $p \leq 0.01$, t test) between CTR and the HLHS line depicted in the same color. **(C)** Representative traces of contraction force at increasing stimulation frequencies in one control and one HLHS line from an experiment aimed at assessing the force-frequency relationship and the paceability at different stimulation frequencies. Stimulation pulses are indicated as vertical bars above the respective tracing. **(D)** Percentage of patches responding to stimulation

at different indicated pacing frequencies. Data are mean ± SEM, n ≥ 3 patches/cell line, ** p ≤ 0.01, chi-squared test. **(E)** Statistical analysis of force-frequency relationship FFR) obtained from HLHS and control patches at different indicated time points are shown. Data are mean ± SEM, n ≥ 3 patches/cell line, ** p ≤ 0.01, t test) compared to CTR on D7.

The phenomenon of reduced paceability of HLHS heart patches correlated with cellular Ca^{2+} measurements that showed a reduced number of paceable cells together with a decline in the number of electrically responsive HLHS-CMs within the patch at higher pacing frequencies (Figure 14B) on day 24. Furthermore, cellular calcium transient amplitudes displayed similar values in HLHS and control cell lines at lower frequencies (0.5 Hz) but significantly diverged at 1.0 and 1.5 Hz, with an increase of calcium amplitude in control and a decline of calcium amplitude in the HLHS cell lines. Interestingly, this observation was seen together with an increase of the diastolic calcium level in HLHS cell lines that aggravated at higher stimulation frequency. (Figure 14D)

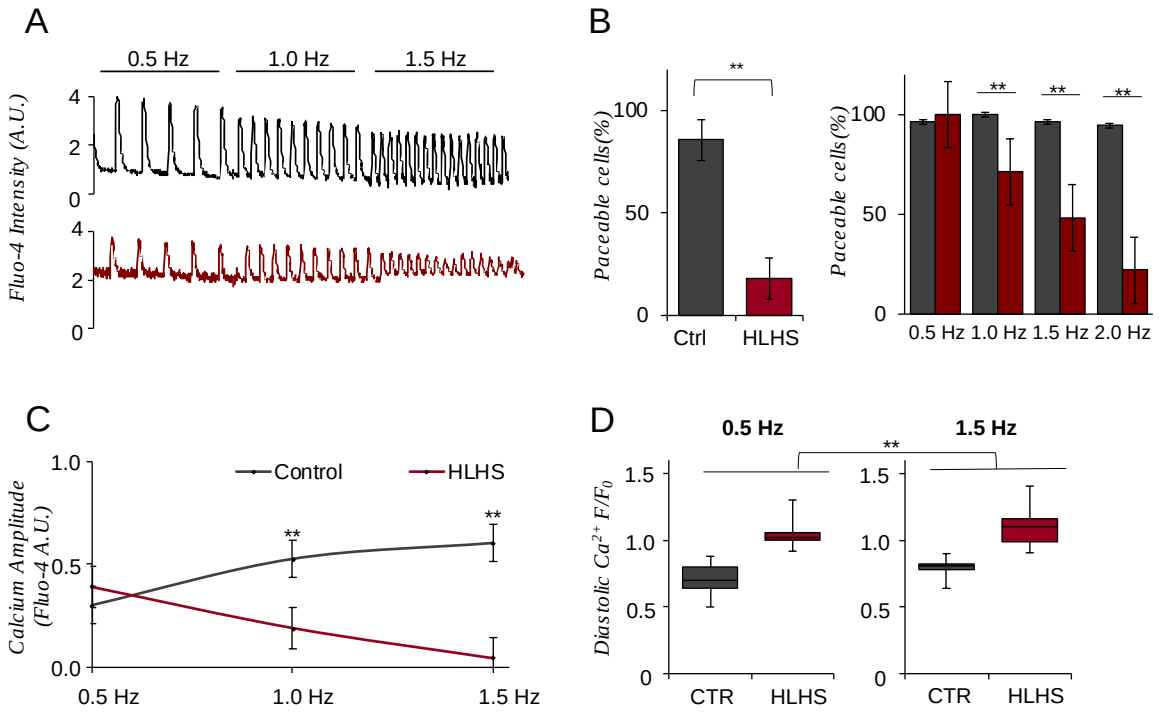

Figure 14. HLHS iPSC-CMs develop increased diastolic calcium levels and display reduced paceability on day 24 of BMC. (A) Representative images of Fluo-4-based intracellular calcium transients from single control and HLHS CMs within the patch at increasing pacing rates. Vertical bars over the tracings represent the stimulation pulses. Data

are shown in arbitrary units (A.U.) **(B)** Left, overall percentage of paceable CMs within control and HLHS heart patches on day 24 of BMC. Right, statistical analysis considering only cells that were paceable showing the percentage of cells responding to the indicated frequency on day 24. Data are mean ± SEM, n ≥ 3 patches/cell line, ** p ≤ 0.01, chi-squared test. **(C)** Amplitude of the systolic calcium transients shown as a function of the stimulation frequency for CMs within control and HLHS patches on day 24 of BMC. **(D)** Diastolic calcium level (shown as ratio of the diastolic Fluo-4 intensity at the indicated pacing frequency (F) and the basal Fluo-4 intensity at the beginning of the experiment (F0)) of single CMs within control and HLHS patches at 0.5 Hz and 1.5 Hz pacing rates on day 24. Data are mean ± SEM, n ≥ 3 patches/cell line, ** p<0.05, t test.

7.6 INCREASED CELL DEATH OF HLHS HIPSC-CMS UNDER BIOMIMETIC CONDITIONS

To investigate the cause of the gradual decline in contraction force and paceability of diseased hiPSC-CMs, a dynamic evaluation of cell viability was performed using an ethidium dimer and calcein-based cell viability assay. Thereby, an increased rate of cellular death was seen in the HLHS 3D heart patches.
During the culture period of 24 days, patches were subjected to the viability assay on days 5, 15 and 24 after initiation of 3D BMC. Corresponding to the decline of contraction force, an increased number of dead cells was observed with a striking difference between control and HLHS cell lines. (Figure 15A)

A major limitation of this assay is that it does not exclusively mark cardiomyocytes inside the 3D cECM heart patch, leaving the risk of also marking fibroblasts or other cell types within the 3D construct. To exclude this possibility, cardiac patches were cryosectioned and immunostained for cardiac troponin T and a combination of two apoptotic markers, namely TUNEL that is based on the incorporation of modified dUTPs at the 3′-OH ends of fragmented DNA, and cleaved caspase 3 that is directly involved in the cellular apoptosis pathway (Figure 15B). This analysis showed a significant difference in apoptotic cardiomyocytes between the HLHS-cardiomyocyte cohort and control hiPSC-CMs. (Figure 15C). 58% ± 5.1 of cell nuclei in HLHS hiPSC-CMs were positive for the apoptosis marker TUNEL, whereas only 14% ± 1.8 of cell nuclei were positive for TUNEL in the control samples on day 24.

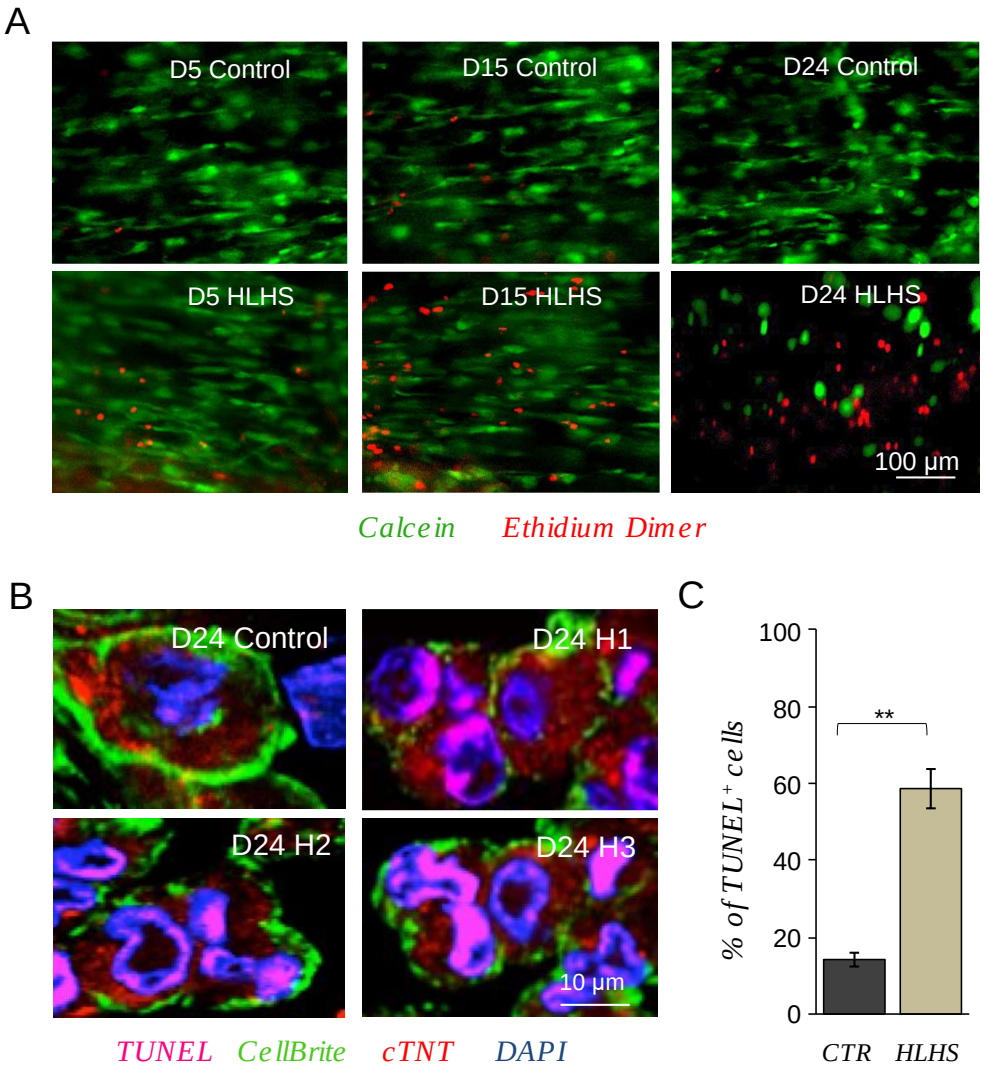

Figure 15. Progressive cell death in the 3D cECM heart patch due to apoptosis of HLHS hiPSC-CM. (A) Representative images of dynamic evaluation of cell death with calcein (life cells) and Ethidium Dimer (dead cells) based cell viability assay on days 5, 15 and 24 in control and HLHS cell lines. **(B)** Representative immunofluorescence analysis for hiPSC-CM cell death showing TUNEL labeling together with cardiac troponin T (cTnT) and CellBright for cell border localization on day 24 in control and HLHS conditions. (C) Statistical analysis of TUNEL positivity within control and HLHS patches. Data are shown as mean ± SEM, n = ≥ 120 cells/patch, ** $p<0.05$, t-test.

Careful analysis of apoptotic cell nuclei revealed an interesting unique phenotype of multinucleation that was evident in all three patient lines but present to a much lesser extent in control hiPSC-CMs. Statistical analysis revealed a significant multinucleation defined by >2 cell nuclei/cell. Immunofluorescent analysis cell nuclei (using Z-stack analysis) displayed

that 26% ± 1.24 of HLHS patient samples had four cell nuclei, 22% ± 2.16 had three cell nuclei, 18% ± 0.94 were binucleated and 34% ± 3.55 mononucleated. The rate of multinucleation in HLHS hiPSC-CM deviated significantly from control samples, where 69% ± 2.05 had one cell nucleus, 26% ± 4.08 were binucleated, 4% ± 2.44 trinucleated, and none had four cell nuclei (Figure 16A).

To further investigate this phenotype of multinucleation, the correlation between multinucleation and apoptosis was addressed by investigating the percentage of TUNEL positive cell nuclei with respect to cell nuclei number.
This sub analysis revealed that the majority of apoptotic cells had 3 or more cell nuclei with a significantly higher occurrence in all HLHS cell lines compared to control-hiPSC-CMs. (Figure 16B)

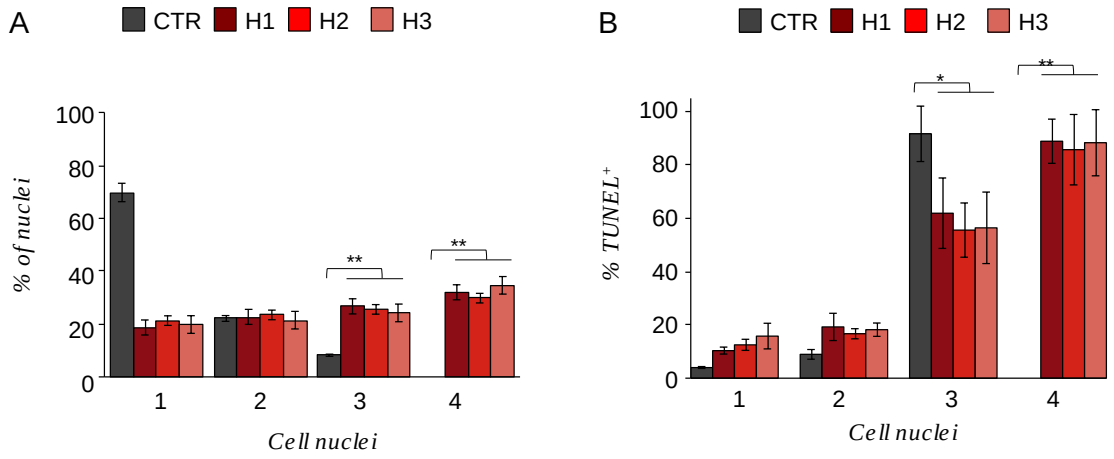

Figure 16. Apoptosis and multinucleation as distinct phenotype of HLHS hiPSC-CMs. **(A)** Statistical analysis of multinucleation in control and HLHS cell lines on day 24 subjected to 3D biomimetic culture. **(B)** Statistical analysis for correlation of multinucleation and apoptosis (% $TUNEL^{+}$) with respect to number of cell nuclei. Data indicated as mean ± SEM, n ≥ 123 cell nuclei/group * $p \leq 0.05$ ** $p \leq 0.01$, t-test.

7.7 HLHS HIPSC-CMS EXHIBIT THINNED SARCOMERES WITH REDUCED RESPONSE TO MECHANICAL LOAD

3D cECM heart patches were analyzed for sarcomeric structures on day 10 in 3D culture before patches were subjected to BMC to dissect the role of mechanical load on HLHS

disease phenotype and progression. Immunofluorescent analysis revealed thin and unorganized sarcomeres on D10 in control and HLHS 3D heart patches. (Figure 17A) Although control CMs appeared to benefit from biomimetic culture with respect to sarcomeric alignment and thickness, HLHS cardiomyocytes displayed impaired sarcomere maturation and failed to develop oriented, aligned and thickened sarcomeres after subjection to mechanical load and electrical stimulation within BMCC. (Figure 17B)

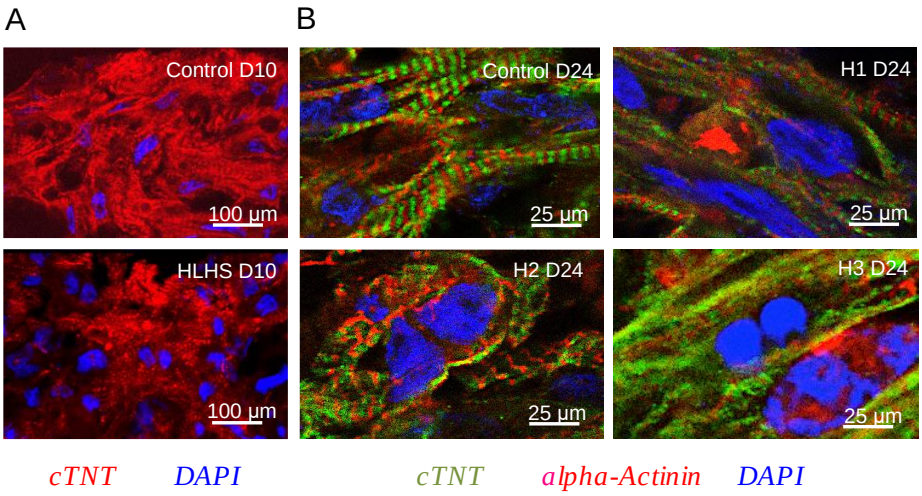

Figure 17. HLHS-CMs exhibit thinned sarcomeres in 3D biomimetic culture. (A) Representative immunostainings for cardiac Troponin T (cTNT) in control and HLHS samples on day 10 without BMC conditions and **(B)** combination of cTNT with alpha actinin for sarcomere visualization on day 24 of BMC in HLHS and control cell lines.

7.8 HLHS-CMs PRIMARILY ADAPT ATRIAL AND IMMATURE CARDIOMYOCYTE PHENOTYPE

To further dissect the cellular maturation of control and HLHS hiPSC-CMs under 3D biomimetic culture conditions, immunofluorescence analysis of atrial and ventricular isoforms of the myosin light chain (MLC2a and MLC2v) was performed. (Figure 17A)
While exclusive MLC2v expression defines maturing ventricular cardiomyocytes, MLC2a is expressed in all immature CMs before it becomes specific for atrial cells during cardiac development.

Analysis on days 12 and 24 of control hiPSC-CMs revealed a high proportion of ventricular cardiomyocytes already on day 12 of BMC (71.94% ± 4.67) that further increased to 81.21%

± 7.64 by day 24. Likewise, a reduction of MLC2a expression between day 12 (5.85% ± 1.84) and day 24 (9.9% ± 2.54) occurred.

In HLHS patches, a striking increase of $MLC2a^+$ cells at the cost of $MLC2v^+$ CMs was observed on days 12 and 24. Most interestingly, the expression of MLC2a in all three HLHS patient lines displayed a significantly increased proportion of MLC2a-positive cells already on day 12 (62.67% ± 1.03) that further increased to 64% ± 3.96 by day 24.

Furthermore, the proportion of MLC2a and MLC2v double-positive cells, that were classified as immature cells, decreased in the control groups from 22.23% ± 7.54 on day 12 to 8.86% ± 2.54 on day 24, whereas the proportion of double-positive cells increased from 19.78% ± 5.21 on day 12 to 32.48% ± 7.42 on day 24 in all patient cell lines. (Figure 17B)

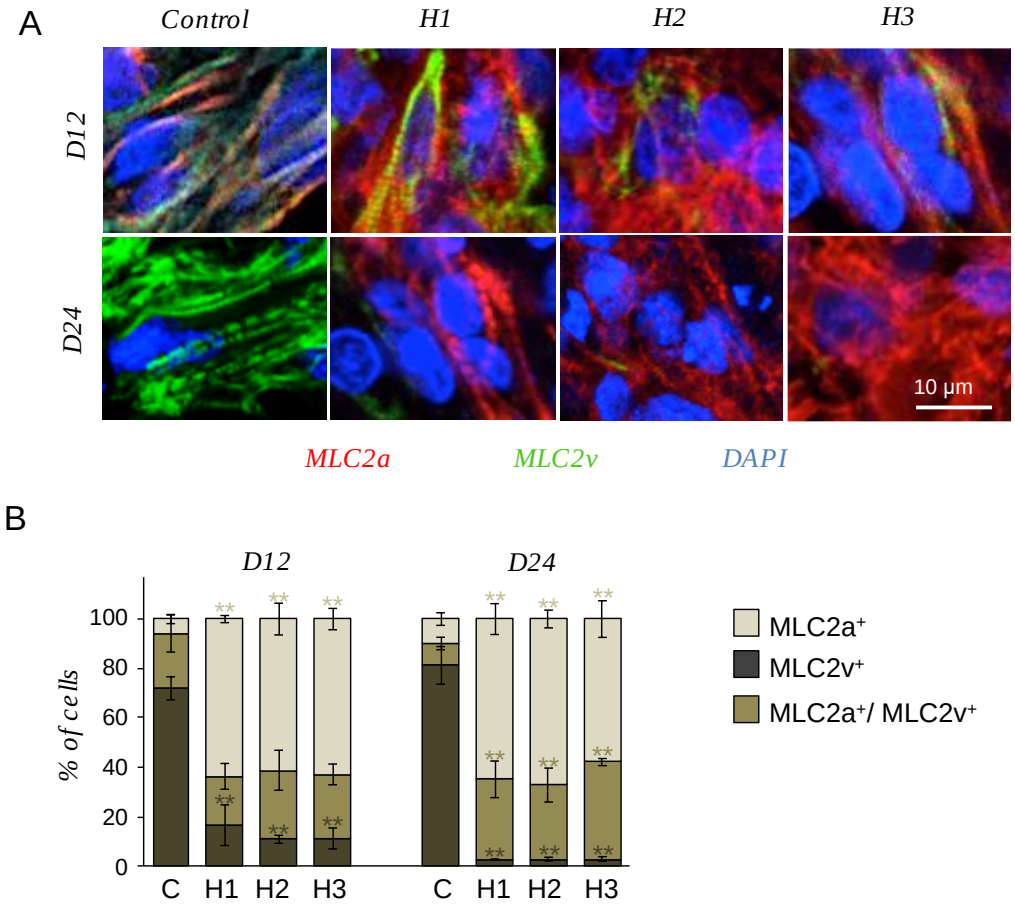

Figure 18. HLHS hiPSC-CMs primarily adapt atrial and immature phenotype within 3D cECM heart patches. **(A)** Representative immunofluorescence stainings for MLC2a (atrial/immature CMs), MLC2v (maturing ventricular CMs) and DAPI of control and HLHS samples on days 12 and 24 of BMC. **(B)** Statistical analysis of cell type specification showing

the percentage of cells exclusively expressing MLC2a or MLC2v or cells with a co-expression of MLC2a/MLC2a. Data are shown as mean ± SEM, n ≥ 190 cells/cell line, color-coded asterisks indicate significant differences between CTR and the HLHS line depicted in the same color, ** $p \leq 0.01$, chi-squared test.

8 DISCUSSION

8.1 CECM ENABLES LONG-TERM 3D CULTURE AND PROVIDES AN EXPERIMENTAL SYSTEM FOR HIPSC-CMS

In the current thesis, it is hypothesized that the native extracellular matrix of non-human primate hearts provides a 3D culture system for hiPSC-CMs while it simultaneously functions as an experimental system to study disease phenotypes such as hypoplastic left heart syndrome (HLHS).
It is furthermore hypothesized that the cECM, with respect to native stiffness and protein components, favors the structural and functional improvement of hiPSC-CM. The results, obtained from a culture period of 40 days, revealed that maturation in the 3D environment is enhanced compared to standard 2D culture. Most of the CMs inside the ECM displayed an elongated cell shape and aligned sarcomeres. (Figure 12) Moreover, maturation with cell type specification towards ventricular cardiomyocytes was observed (Figure 18) together with electrical maturation, as assessed by calcium handling properties and force-frequency-relationship. (Figure 13)

In recent years, the field of 3D tissue engineering in cardiovascular research has already led to major improvements in cellular maturation. The majority of engineered heart tissues are based on chemically defined or naturally obtained extracellular matrix proteins used to create newly formed scaffolds that surround the cells.
These models served as a basis for the developed 3D cECM heart patches as they are all based on extracellular matrix proteins that have proven beneficial for the maturation of hiPSC-CMs. Nonetheless, an important advantage of the native extracellular matrix, besides their isolated components, is the existing functional architecture with the required tissue elasticity.
The intact cardiac ECM scaffold can promote parallel cell alignment and guide cell orientation and elongation along the pre-existent matrix fiber direction.(David L. Andrews, Gregory D. Scholes, 2010). The cECM resembles an elastic tissue that allows cellular contractions while ensuring a firm anchorage. Research has shown that substrate stiffness alone can affect the differentiation of mesenchymal stem cells into myogenic cells, alter cell morphology and differentiation.(Jacot et al., 2010; Macrí-Pellizzeri et al., 2015)
Moreover, it is known that mechanical strain on embryonic stem cells promotes cardiomyogenesis(Gwak et al., 2008) and mechanical loading has a direct effect on CM

differentiation and cell type specification (Shimko & Claycomb, 2008) that leads to an improved contraction force.(Engler et al., 2008)

Further on, mechanical load was not only applied by the surrounding cECM scaffold, but additionally the application of a physiologic preload by the custom- built biomimetic chambers (Fischer et al., 2019) was possible. Described EHT models are commonly attached to micro-posts or pillars with known strength that promotes cell alignment and orientation. (Weinberger et al., 2018, Zimmermann et al., 2006, Hansen et al., 2010, Nunes et al., 2013) However, one major advantage of the used BMC is that the preload can be individually adjusted for each construct; dependent on size, cell number and strength. Feedback of dynamic preload levels (in mN) enables a precise application of physiologic preload that can be adjusted throughout the culture period. Another benefit of the biomimetic culture conditions of the 3D cECM heart patches is the ability to continuously and non-invasively measure contractile force and electrical measurements like FFR.

Consecutively, the generation of contractile force is a major criterion for functional cardiac tissue and the reached contractile performance of 3D cECM heart patches exceeded the contractile force of reported comparable 3D tissue engineered construct (Radisic et al., 2004, Mannhardt et al., 2016, Zhao et al., 2019)

8.1.1 Electrical maturation of hiPSC-CMs in 3D cECM heart patches

Many studies have pointed out the beneficial effects of electrical stimulation on the maturation of immature hiPSC-CMs. Distinct experiments of hiPSC-CM within Biowires (Nunes et al., 2013) and neonatal rat ventricular cells within collagen scaffolds (Radisic et al., 2004) applied electrical field stimulation on cells in 3D cell culture ranging from 1 Hz to suprathreshold stimulation. Increased cell elongation and ultrastructural organization of cells on the one hand and a promoted alignment and coupling of cells on the other hand were observed. Surprisingly, cardiac maturation was shown to be dependent on stimulation rate, revealing the best maturational drive at a stimulation rate of 6 Hz.(Seth, 2013)

A recent study of Ronaldson et al. demonstrated a similar approach of hiPSC-CM cell maturation using 3D tissue engineering together with the application of electrical stimulation. It was shown that frequent cellular stimulations at up to 6 Hz dramatically increased electrical

maturation in terms of connexin- formation when applied to D14 cardiomyocytes (Ronaldson et al., 2018)

These results are in line with the described observations in this study. However, instead of once-daily stimulation, continuous electrical pacing was applied, leading to comparable levels of electromechanical maturation and furthermore the development of a positive force-frequency relationship was reached, a hallmark of maturation that is hardly achieved in 3D cardiac tissue engineering. (Feric et al., 2016, Yang et al., 2014) an only recently has been described in a study of Ronaldson-Bouchard et al. In this work, the authors demonstrated an enhanced development of mature ultrastructure and function by high intensity conditioning of 3D engineered heart tissue where constructs that were subjected to increased stimulation frequencies (0.33 Hz/day; from 2-6 Hz) during a culture period of 4 weeks. (Ronaldson-Bouchard et al., 2018) Weather a long-term intensity training between 2-6 Hz will further enhance the cellular maturation of hiPSC-CM within 3D cECM heart patches needs to be investigated.

8.1.2 Structural maturation of hiPSC-CMs in 3D cECM heart patches

Structural maturation is directly linked to cell performance, as an elongated cell shape is essential for proper force generation. Previous 2D studies have shown that cell shape improvement can also be accomplished in 2D conditions, achieved by long-term culture. Lundy et al. showed that on the basis of 2D culture on glass coverslips, early-stage hESC-CMs (20–40 days in 2D culture) were structurally similar to late-stage hiPSC-CMs (80–120 days in 2D culture). Early-stage CMs exhibited poor subcellular organization and structural alignment, whereas after 3–4 months in culture, cells gradually increased in terms of sarcomeric organization and cell body length.(Lundy et al., 2013)

In the current work, significant cellular alignment and elongation in the majority of cardiomyocytes inside 3D cECM heart patches was already observed after 1 month in BMC. This is also shown by the abundant appearance of ventricular isoform of myosin light chain (MLC2v) and contractile performance on day 24 (Figure 19). Reported results from Zhao et al. suggest that the majority of cellular maturation and adaption of a ventricular phenotype of hiPSC-CMs is achieved by combining 3D tissue engineering with electrical field conditioning. (Zhao et al. 2019)

8.2 RECAPITULATION OF HLHS PHENOTYPE INSIDE 3D CECM HEART PATCHES

Human cardiac diseases, in particular, complex, multi-genetic diseases such as hypoplastic left heart syndrome, have been the subject of numerous in vivo and in vitro studies to investigate and identify major disease-causing factors.(Gaber et al., 2013; Liu et al., 2017b; Yagi et al., 2018)
With the 3D cECM heart patch, an experimental setup that allows sufficient cellular maturation by closely resembling physiologic conditions was generated. With this tool, disease-specific phenotype features arising from diseased HLHS hiPSC- CMs were investigated.

8.2.1 CELL IDENTITY DEFECTS OF HLHS HIPSC-CMS

Previous 2D experiments in our lab have shown an increased presence of MLC2a-expressing cardiomyocytes in HLHS hiPSC-CMs up to differential day 40 or later when compared to control cell lines. These results are in line with several studies that claim a persistent expression of embryonic genes in HLHS cardiomyocytes, indicating a premature state of those patient cells.(Bohlmeyer et al., 2003) However, further maturation of hiPSC-CM in vitro is required to allow the distinction between immaturity and cell type specification.(Zhang et al. 2012)

As demonstrated in the results section, a shift in MLC2a expression from day 12 to day 24 in the control group with an increase in the ventricular phenotype (MLC2v expression) was observed. An interesting consideration in the context of cell-type specification is that analysis on days 12 and 24 for MLC2a and MLC2v in fact revealed 3 distinct patterns: (1) MLC2a-only expressing CMs, (2) MLC2v-only expressing CMs, (3) MLC2a and MLC2v co-expressing (double^{+}) cells.
The obtained results are not only indicative of the predominant adaption of an atrial phenotype but also of an increased population of HLHS hiPSC-CMs that stay in a transient, undefined, and thus immature cell state. Moreover, based on the expression of specific cardiac markers during iPSC differentiation, previous studies suggested defective cellular commitment to the ventricular lineage in HLHS.(Kobayashi et al., 2014; JIANG et al., 2013)

8.2.2 CELL-CYCLE DEFECTS AND APOPTOSIS OF HLHS HIPSC-CMS

The progressive loss of contractile performance of 3D HLHS heart patches was thought to be primarily caused by progressive cell death, as indicated by the dynamic evaluation of cell viability (Figure 15). Detailed analysis using TUNEL assay confirmed a progressive apoptotic cell death of HLHS cardiomyocytes. These results are supported by a study that demonstrated increased apoptosis in native HLHS LV tissue samples.(Liu et al., 2017a)

Surprisingly, the occurrence of apoptosis was lined to an increased rate of multinucleation. In previous studies of HLHS cardiomyocytes, increased cell death was seen together with intrinsic cell cycle defects.(Liu et al., 2017a; Yagi et al., 2018) Furthermore, microarray analysis of native HLHS hearts performed by Gambetta et al. demonstrated an altered expression of several cell cycle regulators that presumably block cell cycle progression and can thus lead to apoptosis.(Gambetta et al., 2008)

Nonetheless, further evaluations using cell-cycle markers such as Ki67 and PH3 that mark distinct stages of the cell cycle are needed for cell-cycle analysis and are the objective of ongoing studies. Similarly, the investigation of underlying mechanisms that lead to the increased occurrence of cell death in HLHS patient cardiomyocytes has to be addressed in a more detailed analysis.

Most interestingly, increased cell death and multinucleation were seen only when cells were subjected to 3D biomimetic culture conditions with continuous electric field stimulation and the application of physiologic preload. Demonstrated immunostainings for sarcomeric structures are suggestive of the fact that HLHS cardiomyocytes are more susceptible to physiologic stress. In the situation where these cells are prone to produce significant contractile performance, they might fail to respond physiologically and instead respond with increased cell-cycle activity and apoptosis.

8.3 Limitations of the studies and Future approaches to deciphering pathogenic alterations of the HLHS phenotype

The recapitulation of the HLHS phenotype in a cellular model using patient-specific HLHS hiPSC-CMs has the advantage of allowing single-cell resolution for molecular studies. Furthermore, the analysis in a 3D syncytium bears the potential to not only study cells in an isolated surrounding but also understand their syncytial behavior on an electrophysiologic and arrhythmogenic perspective. With the application of our 3D biomimetic culture chambers, a direct readout of contraction force performance is possible, allowing to monitor responses to different pacing frequencies and conditions.

However, for studying disease phenotypes, further Ca^{2+} imaging for excitation–contraction studies and the investigation of calcium wave propagation could be beneficial for electrophysiological evaluation. These analyses would also allow the identification of altered calcium-handling properties underlying many congenital heart diseases.

Furthermore, as indicated previously, a more detailed analysis of cell-cycle defects is needed. By marking the several stages of cell cycles using specific immunofluorescent markers, the analysis of cell-cycle delay or alterations would give valuable information about intrinsic cardiomyocyte defects that can be specifically attributed to HLHS cardiomyocytes.

9 SUMMARY AND CONCLUSION

The aim of this study was to provide guidance for the successful reseeding of acellularized NHP heart tissue, demonstrating the generation of a 3D culture system for hiPSC-CMs with optimized culture conditions and ideal maturational support. The obtained results are an encouraging example of the potential role of the native extracellular matrix as a scaffold together with the beneficial effects of biomimetic culture conditions.

With the potential to overcome hiPSC-CM immaturity to a certain degree and by subjecting the cells to electromechnical conditioning in a 3D environment, the recapitulation of the HLHS phenotype in an in vitro setting, by provoking pathognomonic reactions in response to cues for cell division, growth and maturation, was possible.

The obtained results permit to assume that an intrinsic defect of ventricular CM lineage specification and the elevated rate of apoptosis might play a role in disease onset and progression. Thus, it can be hypothesized that the hypoplastic left ventricle in HLHS is not exclusively a consequence of disrupted valve formation and impaired blood flow.

This work demonstrates, that studying cardiac developmental processes in patients with congenital heart diseases outside in vivo settings is possible and might allow a deeper understanding of pathophysiological changes on cellular and sub-cellular levels using the established 3D culture system.

Alessandra Moretti, P. D., Milena Bellin, P. D., Andrea Welling, P. D., Christian Billy Jung, M. S., Jason T. Lam, P. D., Lorenz Bott-Flügel, M. D., Tatjana Dorn, P. D., Alexander Goedel, M. D., Christian Höhnke, M. D., Franz Hofmann, M. D., Melchior Seyfarth, M. D., Daniel Sinnecker, M. D., Albert Schömig, M. D., & Karl-Ludwig Laugwitz, M. D. (2010). Patient-Specific Induced Pluripotent Stem-Cell Models for Long-QT Syndrome *New England Journal of Medicine*, 307–319. https://doi.org/10.1056/NEJMoa1203165

Biesecker, L. G., Mullikin, J. C., Facio, F. M., Turner, C., Cherukuri, P. F., Blakesley, R. W., Bouffard, G. G., Chines, P. S., Cruz, P., Hansen, N. F., Teer, J. K., Maskeri, B., Young, A. C., NISC Comparative Sequencing Program, M., Manolio, T. A., Wilson, A. F., Finkel, T., Hwang, P., Arai, A., … Green, E. D. (2009). The ClinSeq Project: piloting large-scale genome sequencing for research in genomic medicine. *Genome Research*, *19*(9), 1665–1674. https://doi.org/10.1101/gr.092841.109

Bohlmeyer, T. J., Helmke, S., Ge, S., Lynch, J., Brodsky, G., Sederberg, J. H., Robertson, A. D., Minobe, W., Bristow, M. R., & Perryman, M. B. (2003). Hypoplastic left heart syndrome myocytes are differentiated but possess a unique phenotype. *Cardiovascular Pathology*, *12*(1), 23–31. https://doi.org/10.1016/S1054-8807(02)00127-8

Breckwoldt, K., Letuffe-Brenière, D., Mannhardt, I., Schulze, T., Ulmer, B., Werner, T., Benzin, A., Klampe, B., Reinsch, M. C., Laufer, S., Shibamiya, A., Prondzynski, M., Mearini, G., Schade, D., Fuchs, S., Neuber, C., Krämer, E., Saleem, U., Schulze, M. L., … Hansen, A. (2017). Differentiation of cardiomyocytes and generation of human engineered heart tissue. *Nature Protocols*, *12*, 1177. https://doi.org/10.1038/nprot.2017.033

Burgo, A., Proux-Gillardeaux, V., Sotirakis, E., Bun, P., Casano, A., Verraes, A., Liem, R., Formstecher, E., Coppey-Moisan, M., & Galli, T. (2012). A Molecular Network for the Transport of the TI-VAMP/VAMP7 Vesicles From Cell Center to Periphery. *Developmental Cell*, *23*(1). https://doi.org/10.1016/J.DEVCEL.2012.04.019

Burridge, P. W., Matsa, E., Shukla, P., Lin, Z. C., Churko, J. M., Ebert, A. D., Lan, F.,

Diecke, S., Huber, B., Mordwinkin, N. M., Plews, J. R., Abilez, O. J., Cui, B., Gold, J. D., & Wu, J. C. (2014). Chemically defined generation of human cardiomyocytes. *Nature Methods*, *11*(8), 855–860. https://doi.org/10.1038/nmeth.2999

Camelliti, P., Borg, T., & Kohl, P. (2005). Structural and functional characterisation of cardiac fibroblasts. *Cardiovascular Research*, *65*(1), 40–51. https://doi.org/10.1016/j.cardiores.2004.08.020

Chen, Z., Xian, W., Bellin, M., Dorn, T., Tian, Q., Goedel, A., Dreizehnter, L., Schneider, C. M., Ward-Van Oostwaard, D., Ng, J. K. M., Hinkel, R., Pane, L. S., Mummery, C. L., Lipp, P., Moretti, A., Laugwitz, K. L., & Sinnecker, D. (2017). Subtype-specific promoter-driven action potential imaging for precise disease modelling and drug testing in hiPSC-derived cardiomyocytes. *European Heart Journal*, *38*(4), 292–301. https://doi.org/10.1093/eurheartj/ehw189

Cortes, D., McTiernan, C. D., Ruel, M., Franco, W., Chu, C., Liang, W., Suuronen, E. J., & Alarcon, E. I. (2020). BEaTS-α an open access 3D printed device for in vitro electromechanical stimulation of human induced pluripotent stem cells. *Scientific Reports*, *10*(1), 11274. https://doi.org/10.1038/s41598-020-67169-1

Crucean, A., Alqahtani, A., Barron, D. J., Brawn, W. J., Richardson, R. V., O'Sullivan, J., Anderson, R. H., Henderson, D. J., & Chaudhry, B. (2017). Re-evaluation of hypoplastic left heart syndrome from a developmental and morphological perspective. *Orphanet Journal of Rare Diseases*, *12*(1), 138. https://doi.org/10.1186/s13023-017-0683-4

David L. Andrews, Gregory D. Scholes, G. P. W. (2010). *Comprehensive Nanoscience and Technology, Five-Volume set*. Academic Press. https://books.google.com/books?id=Qx-l7MaM3XAC&pgis=1

Donghui Zhang, Ilya Shadrin, Jason Lam, Hai-Qian Xian, R., & Snodgrass, N. B. (2011). *Tissue-engineered Cardiac Patch for Advanced Functional Maturation of Human ESC-derived Cardiomyocytes*. *72*(2), 181–204. https://doi.org/10.1038/nature13314.A

Dorn, T., Kornherr, J., Parrotta, E. I., Zawada, D., Ayetey, H., Santamaria, G., Iop, L.,

Mastantuono, E., Sinnecker, D., Goedel, A., Dirschinger, R. J., My, I., Laue, S., Bozoglu, T., Baarlink, C., Ziegler, T., Graf, E., Hinkel, R., Cuda, G., … Moretti, A. (2018). Interplay of cell–cell contacts and RhoA/MRTF-A signaling regulates cardiomyocyte identity. *The EMBO Journal*, *37*(12), e98133. https://doi.org/10.15252/embj.201798133

Ellen Poon, Chi-wing Kong, R. A. L. (2013). Human Pluripotent Stem Cell-Based Approaches for Myocardial Repair: From the Electrophysiological Perspective. *Mol Pharmaceut 2011, 8:1495–1504.*, *18*(9), 1199–1216. https://doi.org/10.1016/j.micinf.2011.07.011.Innate

Engler, A. J., Carag-Krieger, C., Johnson, C. P., Raab, M., Tang, H.-Y., Speicher, D. W., Sanger, J. W., Sanger, J. M., & Discher, D. E. (2008). Embryonic cardiomyocytes beat best on a matrix with heart-like elasticity: scar-like rigidity inhibits beating. *Journal of Cell Science*, *121*(Pt 22), 3794–3802. https://doi.org/10.1242/jcs.029678

Engler, A. J., Carag-krieger, C., Johnson, C. P., Raab, M., Tang, H., Speicher, D. W., Sanger, J. W., Sanger, J. M., & Discher, E. (2009). *Elasticity : Scar-Like Rigidity Inhibits Beating*. *121*(Pt 22), 3794–3802. https://doi.org/10.1242/jcs.029678.Embryonic

Feaster, T. K., Cadar, A. G., Wang, L., Williams, C. H., Chun, Y. W., Hempel, J., Bloodworth, N., Merryman, W. D., Lim, C. C., Wu, J. C., Knollmann, B. C., & Hong, C. C. (2015). Matrigel Mattress: A Method for the Generation of Single Contracting Human-Induced Pluripotent Stem Cell-Derived Cardiomyocytes. *Circulation Research*, *August*, CIRCRESAHA.115.307580. https://doi.org/10.1161/CIRCRESAHA.115.307580

Feinstein, J. A., Benson, D. W., Dubin, A. M., Cohen, M. S., Maxey, D. M., Mahle, W. T., Pahl, E., Villafañe, J., Bhatt, A. B., Peng, L. F., Johnson, B. A., Marsden, A. L., Daniels, C. J., Rudd, N. A., Caldarone, C. A., Mussatto, K. A., Morales, D. L., Ivy, D. D., Gaynor, J. W., … Martin, G. R. (2012). Hypoplastic Left Heart Syndrome. *Journal of the American College of Cardiology*, *59*(1), S1–S42. https://doi.org/10.1016/j.jacc.2011.09.022

Ferencz, C., Rubin, J. D., McCarter, R. J., Brenner, J. I., Neill, C. A., Perry, L. W., Hepner, S. I., & Downing, J. W. (1985). Congenital heart disease: prevalence at livebirth. The Baltimore-Washington Infant Study. *American Journal of Epidemiology*, *121*(1), 31–36. http://www.ncbi.nlm.nih.gov/pubmed/3964990

Feric NT, Radisic M. Maturing human pluripotent stem cell-derived cardiomyocytes in human engineered cardiac tissues. Adv Drug Deliv Rev. 2016 Jan 15;96:110-34. https://doi: 10.1016/j.addr.2015.04.019

Fischer, C., Milting, H., Fein, E., Reiser, E., Lu, K., Seidel, T., Schinner, C., Schwarzmayr, T., Schramm, R., Tomasi, R., Husse, B., Cao-Ehlker, X., Pohl, U., & Dendorfer, A. (2019). *Long-term functional and structural preservation of precision-cut human myocardium under continuous electromechanical stimulation in vitro*. https://doi.org/10.1038/s41467-018-08003-1

Freud, L. R., McElhinney, D. B., Marshall, A. C., Marx, G. R., Friedman, K. G., del Nido, P. J., Emani, S. M., Lafranchi, T., Silva, V., Wilkins-Haug, L. E., Benson, C. B., Lock, J. E., & Tworetzky, W. (2014). Fetal aortic valvuloplasty for evolving hypoplastic left heart syndrome: postnatal outcomes of the first 100 patients. *Circulation*, *130*(8), 638–645. https://doi.org/10.1161/CIRCULATIONAHA.114.009032

Freytes, Donald O. John D O'Neill, Yi Duan- Arnold, Emily Wrona, and Gordana Vunjak-Novakovic. (2014). Native Cardiac Extracellular Matrix Hydrogels for Cultivation of Human Stem Cell- Derived Cardiomyocytes. *Methods Mol Biol. 2014 ; 1181: 69–81.* https://doi.org/10.1007/978-1-4939-1047-2

Gaber, N., Gagliardi, M., Patel, P., Kinnear, C., Zhang, C., Chitayat, D., Shannon, P., Jaeggi, E., Tabori, U., Keller, G., & Mital, S. (2013). Fetal reprogramming and senescence in hypoplastic left heart syndrome and in human pluripotent stem cells during cardiac differentiation. *American Journal of Pathology*, *183*(3), 720–734. https://doi.org/10.1016/j.ajpath.2013.05.022

Gambetta, K., Al-Ahdab, M. K., Ilbawi, M. N., Hassaniya, N., & Gupta, M. (2008). Transcription repression and blocks in cell cycle progression in hypoplastic left heart

syndrome. *American Journal of Physiology-Heart and Circulatory Physiology*, *294*(5), H2268–H2275. https://doi.org/10.1152/ajpheart.91494.2007

Gillum, R. F. (1994). Epidemiology of congenital heart disease in the United States. *American Heart Journal*, *127*(4 Pt 1), 919–927. http://www.ncbi.nlm.nih.gov/pubmed/8154432

Gwak, S.-J., Bhang, S. H., Kim, I.-K., Kim, S.-S., Cho, S.-W., Jeon, O., Yoo, K. J., Putnam, A. J., & Kim, B.-S. (2008). The effect of cyclic strain on embryonic stem cell-derived cardiomyocytes. *Biomaterials*, *29*(7), 844–856. https://doi.org/10.1016/j.biomaterials.2007.10.050

Hansen, A., Eder, A., Bönstrup, M., Flato, M., Mewe, M., Schaaf, S., Aksehirlioglu, B., Schwörer, A., Uebeler, J., & Eschenhagen, T. (2010). Development of a drug screening platform based on engineered heart tissue. *Circulation Research*, *107*(1), 35–44. https://doi.org/10.1161/CIRCRESAHA.109.211458

Harh, J. Y., Paul, M. H., Gallen, W. J., Friedberg, D. Z., & Kaplan, S. (1973). Experimental production of hypoplastic left heart syndrome in the chick embryo. *The American Journal of Cardiology*, *31*(1), 51–56. http://www.ncbi.nlm.nih.gov/pubmed/4682409

Hirt, M. N., Boeddinghaus, J., Mitchell, A., Schaaf, S., B??rnchen, C., M??ller, C., Schulz, H., Hubner, N., Stenzig, J., Stoehr, A., Neuber, C., Eder, A., Luther, P. K., Hansen, A., & Eschenhagen, T. (2014). Functional improvement and maturation of rat and human engineered heart tissue by chronic electrical stimulation. *Journal of Molecular and Cellular Cardiology*, *74*, 151–161. https://doi.org/10.1016/j.yjmcc.2014.05.009

Hoekstra, M., Mummery, C. L., Wilde, A. A. M., Bezzina, C. R., & Verkerk, A. O. (2012). Induced pluripotent stem cell derived cardiomyocytes as models for cardiac arrhythmias. *Frontiers in Physiology*, *3 AUG*(August), 1–14. https://doi.org/10.3389/fphys.2012.00346

Hoffman, J. I. E., & Kaplan, S. (2002). The incidence of congenital heart disease. *Journal of the American College of Cardiology*, *39*(12), 1890–1900. https://doi.org/10.1016/S0735-1097(02)01886-7

Jacot, J. G., Kita-Matsuo, H., Wei, K. A., Vincent Chen, H., Omens, J. H., Mercola, M., & McCulloch, A. D. (2010). Cardiac Myocyte Force Dvelpoment during Differentiation and maturation. *Annals of the New York Academy of Sciences*, *1188*(1), 121–127. https://doi.org/10.1111/j.1749-6632.2009.05091.x.Cardiac

Jianhua Zhang, Matthew Klos, Gisela F. Wilson, Amanda M. Herman, Xiaojun Lian, Kunil K. Raval, Matthew R. Barron, Luqia Hou, Andrew G. Soerens, Junying Yu, Sean P. Palecek, Gary E. Lyons, James A. Thomson, Todd J. Herron, José Jalife, T. J. (2012). *Extracellular Matrix Promotes Highly Efficient Cardiac Differentiation of Human Pluripotent Stem Cells The Matrix Sandwich Method*. https://doi.org/10.1161/CIRCRESAHA.112

Kattman, S. J., Witty, A. D., Gagliardi, M., Dubois, N. C., Niapour, M., Hotta, A., Ellis, J., & Keller, G. (2011). Stage-specific optimization of activin/nodal and BMP signaling promotes cardiac differentiation of mouse and human pluripotent stem cell lines. *Cell Stem Cell*, *8*(2), 228–240. https://doi.org/10.1016/j.stem.2010.12.008

Kern, J. H., Hayes, C. J., Michler, R. E., Gersony, W. M., & Quaegebeur, J. M. (1997). Survival and risk factor analysis for the Norwood procedure for hypoplastic left heart syndrome. *The American Journal of Cardiology*, *80*(2), 170–174. http://www.ncbi.nlm.nih.gov/pubmed/9230154

Kilang, Y., Aba, A., Tilgner, K., Collin, J., Barta, T., Al-Aama, J. Y., Tesarov, L., Hussain, R., Trafford, A., Kirkwood, G., Sernagor, E., Eleftheriou, C., Przyborski, S., Stojkovic, M., L, M., & Armstrong, L. (2013). *An Induced Pluripotent Stem Cell Model of Hypoplastic Left Heart Syndrome (HLHS) Reveals Multiple Expression and Functional Differences in HLHS-Derived Cardiac Myocytes*. 255–264. https://doi.org/10.1002/stem.1607

Kobayashi, J., Yoshida, M., Tarui, S., Hirata, M., Nagai, Y., Kasahara, S., Naruse, K., Ito, H., Sano, S., & Oh, H. (2014). Directed Differentiation of Patient-Specific Induced Pluripotent Stem Cells Identifies the Transcriptional Repression and Epigenetic Modification of NKX2-5, HAND1, and NOTCH1 in Hypoplastic Left Heart Syndrome.

PLoS ONE, *9*(7), e102796. https://doi.org/10.1371/journal.pone.0102796

Krishnan, A., Samtani, R., Dhanantwari, P., Lee, E., Yamada, S., Shiota, K., Donofrio, M. T., Leatherbury, L., & Lo, C. W. (2014). A detailed comparison of mouse and human cardiac development. *Pediatric Research*, *76*(6), 500–507. https://doi.org/10.1038/pr.2014.128

Lee, Y.-K., Ng, K.-M., Chan, Y.-C., Lai, W.-H., Au, K.-W., Ho, C.-Y. J., Wong, L.-Y., Lau, C.-P., Tse, H.-F., & Siu, C.-W. (2010). Triiodothyronine promotes cardiac differentiation and maturation of embryonic stem cells via the classical genomic pathway. *Molecular Endocrinology (Baltimore, Md.)*, *24*(9), 1728–1736. https://doi.org/10.1210/me.2010-0032

Lerou, P. (2011). Human Pluripotent Stem Cells. In P. H. Schwartz & R. L. Wesselschmidt (Eds.), *Methods in molecular biology (Clifton, N.J.)* (Vol. 767). Humana Press. https://doi.org/10.1007/978-1-61779-201-4

Liang, P., Lan, F., Lee, A. S., Gong, T., Sanchez-Freire, V., Wang, Y., Diecke, S., Sallam, K., Knowles, J. W., Wang, P. J., Nguyen, P. K., Bers, D. M., Robbins, R. C., & Wu, J. C. (2013). Drug screening using a library of human induced pluripotent stem cell-derived cardiomyocytes reveals disease-specific patterns of cardiotoxicity. *Circulation*, *127*(16), 1677–1691. https://doi.org/10.1161/CIRCULATIONAHA.113.001883

Lieu, D. K., Fu, J.-D., Chiamvimonvat, N., Tung, K. C., McNerney, G. P., Huser, T., Keller, G., Kong, C.-W., & Li, R. A. (2013). Mechanism-Based Facilitated Maturation of Human Pluripotent Stem Cell-Derived Cardiomyocytes. *Circulation: Arrhythmia and Electrophysiology*, *6*(1), 191–201. https://doi.org/10.1161/CIRCEP.111.973420

Lieu, P. T. (2015). Reprogramming of Human Fibroblasts with Non-integrating RNA Virus on Feeder-Free or Xeno-Free Conditions. *Methods in Molecular Biology (Clifton, N.J.)*, *1330*, 47–54. https://doi.org/10.1007/978-1-4939-2848-4_5

Liu, X., Yagi, H., Saeed, S., Bais, A. S., Gabriel, G. C., Chen, Z., Peterson, K. A., Li, Y., Schwartz, M. C., Reynolds, W. T., Saydmohammed, M., Gibbs, B., Wu, Y., Devine, W.,

Chatterjee, B., Klena, N. T., Kostka, D., de Mesy Bentley, K. L., Ganapathiraju, M. K., … Lo, C. W. (2017a). The complex genetics of hypoplastic left heart syndrome. *Nature Genetics*, *49*(7), 1152–1159. https://doi.org/10.1038/ng.3870

Liu, X., Yagi, H., Saeed, S., Bais, A. S., Gabriel, G. C., Chen, Z., Peterson, K. A., Li, Y., Schwartz, M. C., Reynolds, W. T., Saydmohammed, M., Gibbs, B., Wu, Y., Devine, W., Chatterjee, B., Klena, N. T., Kostka, D., de Mesy Bentley, K. L., Ganapathiraju, M. K., … Lo, C. W. (2017b). The complex genetics of hypoplastic left heart syndrome. *Nature Genetics*, *49*(7), 1152–1159. https://doi.org/10.1038/ng.3870

Lundy, S. D., Zhu, W.-Z., Regnier, M., & Laflamme, M. A. (2013). Structural and Functional Maturation of Cardiomyocytes Derived from Human Pluripotent Stem Cells. *Stem Cells and Development*, *22*(14), 1991–2002. https://doi.org/10.1089/scd.2012.0490

Macrí-Pellizzeri, L., Pelacho, B., Sancho, A., Iglesias-García, O., Simón-Yarza, A. M., Soriano-Navarro, M., González-Granero, S., García-Verdugo, J. M., De-Juan-Pardo, E. M., & Prosper, F. (2015). Substrate stiffness and composition specifically direct differentiation of induced pluripotent stem cells. *Tissue Engineering. Part A*, *21*(9–10), 1633–1641. https://doi.org/10.1089/ten.TEA.2014.0251

Mäkikallio, K., McElhinney, D. B., Levine, J. C., Marx, G. R., Colan, S. D., Marshall, A. C., Lock, J. E., Marcus, E. N., & Tworetzky, W. (2006). Fetal Aortic Valve Stenosis and the Evolution of Hypoplastic Left Heart Syndrome. *Circulation*, *113*(11), 1401–1405. https://doi.org/10.1161/CIRCULATIONAHA.105.588194

Mali, P., & Cheng, L. (2012). Concise Review: Human Cell Engineering: Cellular Reprogramming and Genome Editing. *STEM CELLS*, *30*(1), 75–81. https://doi.org/10.1002/stem.735

Mandai, M., Watanabe, A., Kurimoto, Y., Hirami, Y., Morinaga, C., Daimon, T., Fujihara, M., Akimaru, H., Sakai, N., Shibata, Y., Terada, M., Nomiya, Y., Tanishima, S., Nakamura, M., Kamao, H., Sugita, S., Onishi, A., Ito, T., Fujita, K., … Takahashi, M. (2017). Autologous Induced Stem-Cell–Derived Retinal Cells for Macular Degeneration. *New England Journal of Medicine*, *376*(11), 1038–1046.

https://doi.org/10.1056/NEJMoa1608368

Mannhardt I, Breckwoldt K, Letuffe-Brenière D, Schaaf S, Schulz H, Neuber C, Benzin A, Werner T, Eder A, Schulze T, Klampe B, Christ T, Hirt MN, Huebner N, Moretti A, Eschenhagen T, Hansen A. Human Engineered Heart Tissue: Analysis of Contractile Force. Stem Cell Reports. 2016 Jul 12;7(1):29-42. https://doi: 10.1016/j.stemcr.2016.04.011.

Martin, B.-J., Mah, K., Eckersley, L., Harder, J., Pockett, C., Schantz, D., Dyck, J., Al Aklabi, M., Rebeyka, I. M., & Ross, D. B. (2017). Hypoplastic Left Heart Syndrome Is Not a Predictor of Worse Intermediate Mortality Post Fontan. *The Annals of Thoracic Surgery*, *104*(6), 2037–2044. https://doi.org/10.1016/j.athoracsur.2017.08.032

Matsuda, T., Takahashi, K., Nariai, T., Ito, T., Takatani, T., Fujio, Y., & Azuma, J. (2005). N-cadherin-mediated cell adhesion determines the plasticity for cell alignment in response to mechanical stretch in cultured cardiomyocytes. *Biochemical and Biophysical Research Communications*, *326*(1), 228–232. https://doi.org/10.1016/j.bbrc.2004.11.019

May-Simera, H. L., Gumerson, J. D., Gao, C., Campos, M., Cologna, S. M., Beyer, T., Boldt, K., Kaya, K. D., Patel, N., Kretschmer, F., Kelley, M. W., Petralia, R. S., Davey, M. G., & Li, T. (2016). Loss of MACF1 Abolishes Ciliogenesis and Disrupts Apicobasal Polarity Establishment in the Retina. *Cell Reports*, *17*(5), 1399–1413. https://doi.org/10.1016/j.celrep.2016.09.089

Michelfelder, E., Gomez, C., Border, W., Gottliebson, W., & Franklin, C. (2005). Predictive Value of Fetal Pulmonary Venous Flow Patterns in Identifying the Need for Atrial Septoplasty in the Newborn With Hypoplastic Left Ventricle. *Circulation*, *112*(19), 2974–2979. https://doi.org/10.1161/CIRCULATIONAHA.105.534180

Morleo, M., & Franco, B. (2019). The Autophagy-Cilia Axis: An Intricate Relationship. *Cells*, *8*(8). https://doi.org/10.3390/CELLS8080905

Mummery, C. L., Zhang, J., Ng, E. S., Elliott, D. A., Elefanty, A. G., & Kamp, T. J. (2012). Differentiation of human embryonic stem cells and induced pluripotent stem cells to

cardiomyocytes: a methods overview. *Circulation Research*, *111*(3), 344–358. https://doi.org/10.1161/CIRCRESAHA.110.227512

Nunes, S. S., Miklas, J. W., Liu, J., Aschar-Sobbi, R., Xiao, Y., Zhang, B., Jiang, J., Massé, S., Gagliardi, M., Hsieh, A., Thavandiran, N., Laflamme, M. A., Nanthakumar, K., Gross, G. J., Backx, P. H., Keller, G., & Radisic, M. (2013). Biowire: a platform for maturation of human pluripotent stem cell-derived cardiomyocytes. *Nature Methods*, *10*(8), 781–787. https://doi.org/10.1038/nmeth.2524

Oberwallner, B., Brodarac, A., Choi, Y. H., Saric, T., Anič, P., Morawietz, L., & Stamm, C. (2014). Preparation of cardiac extracellular matrix scaffolds by decellularization of human myocardium. *Journal of Biomedical Materials Research - Part A*. https://doi.org/10.1002/jbm.a.35000

Pane, L. S., My, I., & Moretti, A. (2016). *induced pluripotent stem cells in regenerative medicine chapter 16*.

Parsa, H., Ronaldson, K., & Vunjak-novakovic, G. (2015). Bioengineering methods for myocardial regeneration ☆. *Advanced Drug Delivery Reviews*, 6–13. https://doi.org/10.1016/j.addr.2015.06.012

Pesevski, Z., Kvasilova, A., Stopkova, T., Nanka, O., Drobna Krejci, E., Buffinton, C., Kockova, R., Eckhardt, A., & Sedmera, D. (2018). Endocardial Fibroelastosis is Secondary to Hemodynamic Alterations in the Chick Embryonic Model of Hypoplastic Left Heart Syndrome. *Developmental Dynamics*, *247*(3), 509–520. https://doi.org/10.1002/dvdy.24521

Poelmann, R., & Gittenberger-de Groot, A. (2018). Hemodynamics in Cardiac Development. *Journal of Cardiovascular Development and Disease*, *5*(4), 54. https://doi.org/10.3390/jcdd5040054

Radisic, M., Park, H., Shing, H., Consi, T., Schoen, F. J., Langer, R., Freed, L. E., & Vunjak-Novakovic, G. (2004). Functional assembly of engineered myocardium by electrical stimulation of cardiac myocytes cultured on scaffolds. *Proceedings of the National*

Academy of Sciences of the United States of America, *101*(52), 18129–18134. https://doi.org/10.1073/pnas.0407817101

Rodriguez, A. G., Han, S. J., Regnier, M., & Sniadecki, N. J. (2011). Substrate stiffness increases twitch power of neonatal cardiomyocytes in correlation with changes in myofibril structure and intracellular calcium. *Biophysical Journal*, *101*(10), 2455–2464. https://doi.org/10.1016/j.bpj.2011.09.057

Ronaldson, K., Ma, S., Yeager, K., Chen, T., Song, L., & Sirabella, D. (2018). Advanced maturation of human cardiac tissue grown from pluripotent stem cells. *Nature*. https://doi.org/10.1038/s41586-018-0016-3

Ronaldson-Bouchard K, Ma SP, Yeager K, Chen T, Song L, Sirabella D, Morikawa K, Teles D, Yazawa M, Vunjak-Novakovic G. Advanced maturation of human cardiac tissue grown from pluripotent stem cells. Nature. 2018 Apr;556(7700):239-243. https://doi: 10.1038/s41586-018-0016-3.

Sadineni, R. T., Kumar, B. S., Chander, N. B., & Boppana, D. M. (2017). Prenatal Sonographic Diagnosis of Hypoplastic Left Heart Syndrome. *International Journal of Applied & Basic Medical Research*, *7*(3), 213–215. https://doi.org/10.4103/ijabmr.IJABMR_389_16

Schwartz, S. D., Regillo, C. D., Lam, B. L., Eliott, D., Rosenfeld, P. J., Gregori, N. Z., Hubschman, J. P., Davis, J. L., Heilwell, G., Spirn, M., Maguire, J., Gay, R., Bateman, J., Ostrick, R. M., Morris, D., Vincent, M., Anglade, E., Del Priore, L. V., & Lanza, R. (2015). Human embryonic stem cell-derived retinal pigment epithelium in patients with age-related macular degeneration and Stargardt's macular dystrophy: Follow-up of two open-label phase 1/2 studies. *The Lancet*, *385*(9967), 509–516. https://doi.org/10.1016/S0140-6736(14)61376-3

Seth, A. (2013). Biowire: a new platform for maturation of human pluripotent stem cell derived cardiomyocytes. *Nature Methods*, *49*(2), 743–750. https://doi.org/10.1167/iovs.07-1072.Complement-Associated

Shimko, V., & Claycomb, W. (2008). Effect of mechanical loading on three-dimensional cultures of embryonic stem cell-derived cardiomyocytes. *Tissue Engineering. Part A*, *14*(1), 49–58. https://doi.org/10.1089/ten.2007.0092.Effect

Spinale, F. G. (2002). Matrix Metalloproteinases: Regulation and Dysregulation in the Failing Heart. *Circulation Research*, *90*(5), 520–530. https://doi.org/10.1161/01.RES.0000013290.12884.A3

Stevens, M. M., & George, J. H. (2005). Exploring and engineering the cell surface interface. *Science (New York, N.Y.)*, *310*(5751), 1135–1138. https://doi.org/10.1126/science.1106587

Takahashi, K., Tanabe, K., Ohnuki, M., Narita, M., Ichisaka, T., Tomoda, K., & Yamanaka, S. (2007). Induction of pluripotent stem cells from adult human fibroblasts by defined factors. *Cell*, *131*(5), 861–872. https://doi.org/10.1016/j.cell.2007.11.019

Tiburcy, M., Hudson, J. E., Balfanz, P., Schlick, S., Meyer, T., Liao, M. L. C., Levent, E., Raad, F., Zeidler, S., Wingender, E., Riegler, J., Wang, M., Gold, J. D., Kehat, I., Wettwer, E., Ravens, U., Dierickx, P., Van Laake, L. W., Goumans, M. J., … Zimmermann, W. H. (2017). Defined engineered human myocardium with advanced maturation for applications in heart failure modeling and repair. *Circulation*, *135*(19), 1832–1847. https://doi.org/10.1161/CIRCULATIONAHA.116.024145

Tzatzalos, E., Abilez, O. J., Shukla, P., & Wu, J. C. (2015). Engineered heart tissues and induced pluripotent stem cells: Macro- and microstructures for disease modeling, drug screening, and translational studies. *Advanced Drug Delivery Reviews*. https://doi.org/10.1016/j.addr.2015.09.010

Ulmer, B. M., Stoehr, A., Schulze, M. L., Patel, S., Gucek, M., Mannhardt, I., Funcke, S., Murphy, E., Eschenhagen, T., & Hansen, A. (2018). Contractile Work Contributes to Maturation of Energy Metabolism in hiPSC-Derived Cardiomyocytes. *Stem Cell Reports*, *10*(3), 834–847. https://doi.org/10.1016/j.stemcr.2018.01.039

Weinberger, F., Reinsch, M., Köse, D., Castro, L., Pecha, S., Hansen, A., & Eschenhagen, T.

(2018). Cardiac repair with engineered heart tissue from human induced pluripotent stem cells. *Naunyn-Schmiedeberg's Archives of Pharmacology*, *391*(November), S29. https://doi.org/10.1007/s00210-018-147-75 LK

Willems, E., Cabral-Teixeira, J., Schade, D., Cai, W., Reeves, P., Bushway, P. J., Lanier, M., Walsh, C., Kirchhausen, T., Izpisua Belmonte, J. C., Cashman, J., & Mercola, M. (2012). Small molecule-mediated TGF-?? type II receptor degradation promotes cardiomyogenesis in embryonic stem cells. *Cell Stem Cell*, *11*(2), 242–252. https://doi.org/10.1016/j.stem.2012.04.025

Yagi, H., Liu, X., Gabriel, G. C., Wu, Y., Peterson, K., Murray, S. A., Aronow, B. J., Martin, L. J., Benson, D. W., & Lo, C. W. (2018). The Genetic Landscape of Hypoplastic Left Heart Syndrome. *Pediatric Cardiology*, *39*(6), 1069–1081. https://doi.org/10.1007/s00246-018-1861-4

Yang, X., Pabon, L., & Murry, C. E. (2014). Engineering Adolescence: Maturation of Human Pluripotent Stem Cell-Derived Cardiomyocytes. *Circulation Research*, *114*(3), 511–523. https://doi.org/10.1161/CIRCRESAHA.114.300558

Yang, Xiulan, Pabon, L., & Murry, C. E. (2014). Engineering adolescence: maturation of human pluripotent stem cell-derived cardiomyocytes. *Circulation Research*, *114*(3), 511–523. https://doi.org/10.1161/CIRCRESAHA.114.300558

Yoshimura, S., Gerondopoulos, A., Linford, A., Rigden, D. J., & Barr, F. A. (2010). Family-wide characterization of the DENN domain Rab GDP-GTP exchange factors. *The Journal of Cell Biology*, *191*(2), 367–381. https://doi.org/10.1083/jcb.201008051

Yu, J., Vodyanik, M. A., Smuga-Otto, K., Antosiewicz-Bourget, J., Frane, J. L., Tian, S., Nie, J., Jonsdottir, G. A., Ruotti, V., Stewart, R., Slukvin, I. I., & Thomson, J. A. (2007). Induced pluripotent stem cell lines derived from human somatic cells. *Science (New York, N.Y.)*, *318*(5858), 1917–1920. https://doi.org/10.1126/science.1151526

Zeevaart, J. G., Wang, L., Thakur, V. V, Leung, C. S., Tirado-, J., Bailey, C. M., Domaoal, R. A., Anderson, K. S., & William, L. (2009). Growth of Engineered Human Myocardium

with Mechanical Loading and Vascular Co-culture. *Circulation Research*, *130*(29), 9492–9499. https://doi.org/10.1021/ja8019214.Optimization

Zengrong Zhu and Danwei Huangfu. (2013). *Human pluripotent stem cells: an emerging model in developmental biology*. https://doi.org/10.1242/dev.086165

Zhang, D., & Pu, W. T. (2018). Exercising engineered heart muscle to maturity. *Nature Reviews Cardiology*, *15*(7), 383–384. https://doi.org/10.1038/s41569-018-0032-x

Zhang, J., Wilson, G. F., Soerens, A. G., Koonce, C. H., Yu, J., Palecek, S. P., Thomson, J. A., & Kamp, T. J. (2009). Functional cardiomyocytes derived from human induced pluripotent stem cells. *Circulation Research*, *104*(4), e30-41. https://doi.org/10.1161/CIRCRESAHA.108.192237

Zhao Y, Rafatian N, Feric NT, Cox BJ, Aschar-Sobbi R, Wang EY, Aggarwal P, Zhang B, Conant G, Ronaldson-Bouchard K, Pahnke A, Protze S, Lee JH, Davenport Huyer L, Jekic D, Wickeler A, Naguib HE, Keller GM, Vunjak-Novakovic G, Broeckel U, Backx PH, Radisic M. A Platform for Generation of Chamber-Specific Cardiac Tissues and Disease Modeling. Cell. 2019 Feb 7;176(4):913-927.e18. https://doi: 10.1016/j.cell.2018.11.042.

Zimmermann, W.-H., Melnychenko, I., Wasmeier, G., Didié, M., Naito, H., Nixdorff, U., Hess, A., Budinsky, L., Brune, K., Michaelis, B., Dhein, S., Schwoerer, A., Ehmke, H., & Eschenhagen, T. (2006). Engineered heart tissue grafts improve systolic and diastolic function in infarcted rat hearts. *Nature Medicine*, *12*(4), 452–458. https://doi.org/10.1038/nm1394

11 ACKNOWLEDGEMENTS

First of all, I would like to thank my advisor, Alessandra Moretti for her support and encouragement. For the possibility to stop by at her office at any time, always finding an open ear and important input. Together with Karl-Ludwig Laugwitz, they gave me the opportunity to join their great team in the lab. I'm very thankful for their guidance, critical questions and ideas.

I would like to express my special appreciation and thanks to my supervisor Daniel Sinnecker. Thank you for gently guiding me and sharing your immense knowledge with me. For the time you spent to correct my thesis, your ideas and suggestions but also your great sense of humor. You are a role model in many ways.

A special thanks to Andreas Dendorfer, for letting me work with your setup and for the continuous support on chambers and electrodes but even more for your advice and support.
To Rabea Hinkel at the Deutsches Primatenzentrum Göttingen, for providing us with NHP tissue.

Thanks to all lab members. Anna, Tatjana, Mary, Gianluca, Franziska, Dorota, Zhifen, Svenja, Hilansi, Fangfang, Jessy, Birgit and Christina. For the great fun inside and outside the lab, chats, advices, patience and help anytime I needed it.
Thank you, Sarah for all the illustrations you made for this thesis.

I want to express my thankfulness to my parents and siblings, Elisabeth, Jakob, Angelika, Martin, Michael and Philipp for continuous encouragements and visits and for not being too disappointed when I didn't answer my phone while I was busy with writing this thesis.

Thank you, Felix, for your understanding, self-less and loving support. Your valuable ideas, the numerous discussions and for proofreading several drafts. Your light-hearted way of seeing things was always the biggest motivation.

Thank you, Christine